Biogas industry: Novel acid gas removal technology using a superacid solvent. Process design, unit specification and feasibility study compared with other existing technologies

Iran Charry Prada, Rodrigo Rivera-Tinoco, Chakib Bouallou

Version of Record: https://www.sciencedirect.com/science/article/pii/S026387621930574X
Manuscript_42fb48d70bef6e2c82f1da780873d523

Biogas industry: Novel acid gas removal technology using a superacid solvent. Process design, unit specification and feasibility study compared with other existing technologies

Iran D. Charry Prada, Rodrigo Rivera-Tinoco* and Chakib Bouallou
MINES ParisTech, PSL – Research University, CES – Centre d'Efficacité Energétique des Systèmes, 60 Bd Saint Michel, 75006 Paris, France

ABSTRACT

A novel purification technology for raw biogas streams is proposed and it is based on the use of a superacid solution within a bubble column reactor. The solvent is a mixture of sulfuric acid ($H_2SO_{4(aq)}$, ≥ 95.0 wt. %) and acetic acid glacial ($CH_3COOH_{(l)}$, ≥99.8 vol. %), both commercial grades. A mixture with a molar ratio of 9/1 for $H_2SO_{4(aq)}$, /$CH_3COOH_{(l)}$ respectively, leads to the interesting physical and chemical absorption properties for biogas treatment.

Process simulations of the technology within a frequently used biomethane production process showed simultaneous capabilities for H_2S elimination, CO_2 absorption and, siloxanes and volatile organic compounds (NMVOCs) complete degradation. A single bubble column reactor was designed for treating 500 Nm^3/h of raw biogas with H_2S content between 400 and 1500 ppmv (dry basis) and for handling a solvent volume flow between 10.23 and 23.39 L/min, depending on the H_2S gas content. Proper functioning and hydrodynamic stability of this unit were evaluated in order to avoid possible issues related to bubbles coalescences or break-up, liquid backmixing and mass transfer limitations.

Comparison of the proposed technology with methanol-based and monoethanolamine ($MEA_{(aq)}$)-based absorption processes allowed proving the low energy demands of the proposed unit and the feasible implementation of the technology.

Keywords: superacid solution, biogas treatment, biomethane, absorption

NOMENCLATURE

Greek letters	
$\mathfrak{D}_{gl}$	Gas diffusivity (m^2/s)
β_0	Drag coefficient ($kg/m^3/s$)
$\mathcal{E}$	Holdup (-)
τ	Residence time (s)
ρ	Density (kg/m3)
μ	Dynamic viscosity (Pa.s)
ϕ	Ratio between the mixing time and the mass transfer time (s/s)
σ	Surface tension (N/m)

Variables	
a_i	Interfacial area (m^2/m^3)
AR_b	Bubbles aspect ratio (m/m)
AR_c	Bubble column aspect ratio (m/m)
A_0	Pre-exponential factor for the Arrhenius law constant ($mol\ s^{-1}\ m^{-2}\ Pa^{-1}$)
Bo	Bodestein number (-)
Bd	Bond number (-)
C_{AS}	Concentration of $H_2SO_{4(aq)}$ (wt. %.)
C_{vm}	Virtual mass coefficient (-)
D	Column diameter (m)
d_o	Orifice gas sparger diameter (m)
d_b	Mean bubbles diameter (m)
Da	Damköhler number (-)
D_H *	Hydraulic diameter of the column (m)
Ea	Activation energy (kJ/mol)
E_{DG}	Gas-phase dispersion coefficient (m^2/s)
E_{DL}	Liquid-phase dispersion coefficient (m^2/s)
Eo	Eötvös number (-)
f_l	Stability factor (-)
F	Gas flow rate (kmol/s)
Fr	Froude number (-)
g	Gravity force (9,8 m/s^2)
h_L	Liquid height in the column (m)
I_f	Ionic force related factor (-)
I	Ionic force (g/L)
K_L	Liquid-phase mass transfer coefficient (m/s)
Mw	Molar mass (kg/kmol)
Pe	Peclet number (-)
P_k	Packing factor (m^2/m^3)
Q	Volumetric flow rate (m^3/s)
Q_m	Mass flow rate (g/s)
T	Temperature (K)
tr_G	Residence time of the gas in the column (s)
r_i	Reaction rate of the *i*-reaction ($mol{\cdot}s^{-1}$)
R	Gas constant ($8.314\ m^3{\cdot}Pa{\cdot}mol^{-1}{\cdot}K^{-1}$)
Re	Reynolds number (-)
U	Superficial velocity (m/s)
U_b	Rise velocity of non-spherical bubbles (m/s)
We	Weber number (-)

Subscripts	
G	Gas phase
L	Liquid phase

1. INTRODUCTION

Nowadays, biogas use has risen as an alternative energy source counterbalancing the dependence on fossil fuels. This gas is produced by fermentation of organic matter, such as primary and secondary agricultural residues, industrial and household waste, and sewage. The significant methane (CH_4) content in raw biogas streams, usually above 40 vol. %, allows either producing biomethane (upgraded biogas above 95 vol. % in CH_4) through an intensive purification treatment, or producing partially purified combustion gas for turbines, engines and boilers (depending on the equipment specifications).

Overall biogas composition depends on the source of the organic matter, as summarized in Table 1. Other components different to methane in biogas streams have rather a negative effect on industrial equipment, combustion processes, emissions quality and the environment, as shown in the same table.

Table 1. Nominal biogas streams compositions and its main components effects

Composition					Effects	References
Component	**Agricultural waste**	**Sewage**	**Landfills and household waste**	**Industrial waste**		
CH_4 (vol %)	50 – 80	50 – 60	50 – 80	50 – 70	- Energetically valuable component	(Boulinguiez and Le Cloirec, 2011; Deublein and Steinhauser, 2010; Huertas et al., 2011; Naskeo Environment, 2009; Swedish Gas Centre, 2012)
CO_2 (vol %)	30 – 50	19 – 33	20 – 50	30 – 50	- Reduction of the calorific value of the gas mixture. - Corrosion source in aqueous solutions. - Degradation of alkaline fuel cells.	
N_2 (vol %)	0 – 1	0 – 1	1 – 40	0 – 1	- Reduction of the calorific value of the gas mixture. - Increase of engine rattling effect.	
O_2 (vol %)	0 – 1	< 0,5	0 – 1	0 – 1	--	
H_2S (mg/Nm³)	3000 – 10000	1000 - 4000	100 – 900	400 – 800	- Corrosion for process equipment and pipes. - SO_2 source after a combustion process. - Catalysts deactivation.	
H_2O (vol %)	~ 6 (330 K)	~ 6 (330 K)	~ 6 (330 K)	~ 6 (330 K)	- Corrosion and condensation of process instruments. - Detriment of fuel cells performance.	
NMVOCs (mg/Nm³)	< 2500	< 1500	< 2500	< 2500	- Most important compounds are the Siloxanes, described below.	
Wobbe Index (kWh/Nm³)	5.0 – 6.1	5.5 – 8.2	4.4	6.6 – 8.2	--	
Siloxanes						
L2 (µg/Nm³)	< 5	~ 40	280 – 6000	< 5	SiO_2 precipitation leading to internal abrasion issues in equipment. Reduction of catalyst performance. Reduction of heat transfer and combustion efficiency of equipment. Problems to living organisms, problems affecting their lungs, liver and central nervous system.	(Arrhenius et al., 2011; Boulinguiez and Le Cloirec, 2011; García et al., 2015; Tansel and Surita, 2014)
D3 (µg/Nm³)	< 30	~ 30	30 – 500	~ 20		
L3 (µg/Nm³)	< 5	~ 110	< 5	< 5		
D4 (µg/Nm³)	< 15	~ 1110	~ 12530	~ 130		
L4 (µg/Nm³)	< 10	~ 100	< 10	~ 10		
D5 (µg/Nm³)	< 10	~ 12000	~ 2500	~ 890		
L5 (µg/Nm³)	< 30	~ 240	< 30	~ 60		
D6(µg/Nm³)	< 5	~ 860	~ 15	~ 30		
L2 (Hexamethyldisiloxane) ; L3 (Octamethyltrisiloxane) ; L4 (Decamethyltetrasiloxane) ; L5 (Dodecamethylpentasiloxane) ; D3 (Hexamethylcyclotrisiloxane) ; D4 (Octamethylcyclotetrasiloxane) ; D5 (Decamethylcyclopentasiloxane) ; D6 (Dodecamethylcyclohexasiloxane)						

In terms of the combustion performance, the low Wobbe Index values for raw biogas (Table 1), as compared to natural gas, confirms the operational need for purification before its further use. The Wobbe index for natural gas sales is approximately 14.50 kWh/Nm^3 (Deublein and Steinhauser, 2010; Eimer, 2014). In addition, environmental regulations establish maximum impurities content in purified combustion gases between 3.3 and 4.0 ppmv for sulfur hydroxide (H_2S) and between 2 and 8 vol. %, for carbon dioxide (CO_2), depending on every country sales gas specifications (Kohl and Nielsen, 1997; Nexant-Chem systems, 2006). Regulations also

apply to sulfur dioxide (SO_2) gas emissions, produced by the H_2S combustion, to a maximum between 4.0 and 133.0 ppmv, depending on the combustion facility location (European Commission, 2015; Kohl and Nielsen, 1997).

Specific content of siloxanes and the non-methane volatile organic compounds (NMVOCs) in biogas streams, resulting from its anthropogenic sources, renders necessary a pretreatment for its separation. Siloxanes are produced by industrial matter degradation, such as hygienic and cosmetic products, food additives and other man-made products. Their chemical structure is consisting of silicon, oxygen and alkyl groups in lineal (Li) or cyclic (Di) arrangements (Table 1). The siloxanes noted as D4 and D8 are normally reported as the most frequently found in the biogas (Soreanu et al., 2011; Tansel and Surita, 2014). Siloxanes oxidation, during the gas combustion, leads to silica particles (SiO_2) precipitation, with a size distribution ranging between 4 and 500 nm, depending on the flame temperature of the combustion chamber. Part of the SiO_2 aggregates precipitate in the combustion chambers and chimneys (below 1200 K), whereas a small fraction of solids remains dispersed in the gas emissions (Tansel and Surita, 2014). Negative effects of precipitated SiO_2 are described in the Table 1.

In wake of the mentioned process specifications and environmental regulations, biogas impurities need to be removed seeking a final energy use. Acid gases (H_2S and CO_2) removal is well known and established in decades, based on natural gas processing. Few of these technologies are however used for an overall biogas upgrading through adsorption and absorption-based separation processes. Commonly used adsorption-based activated carbons normally exhibit capacity around 7 times higher for siloxanes and 4 times higher for NMVOCs as compared to H_2S (Bansal and Goyal, 2005; Ford, 2007; Largitte and Pasquier, 2016), whereas carbon molecular sieves, usually Zeolite 5A – lead to estimated separation capacity around 1.5 times higher for H_2S than for CO_2 and a specific selectivity to siloxanes and NMVOCs (Awe et al., 2017; N. Madox, 1982). Separation by absorption-regeneration scrubbing systems using water, organic solvents (e.g., polyethylene glycol, methanol, N-metyl-2-pyrrolidone and carbonate propylene) or inorganic salts (e.g., $NaHCO_3$, K_2CO_3) in aqueous solutions rely on the gas solubility and therefore separate the heavy compounds, siloxanes, NMVOCs, CO_2 and H_2S as compared to the CH_4; however large recycling volumes usually limit its implementation (Ford, 2007; Kohl and Nielsen, 1997). Recent studies propose the use of alkanolamines aqueous solutions but discarding the idea of a regeneration step while used for biogas upgrading (Abdeen et al., 2016; Tippayawong and Thanompongchart, 2013).

Alternatively, other technologies are rather used to eliminate specific impurities from raw biogas streams, such as membrane separation for CO_2 removal, biological or chemical H_2S desulfurization units and low-temperature siloxanes condensation units, among others. Polymeric membranes are currently implemented for CO_2 removal from pretreated biogas streams, usually achieving between 92 and 97 % pure biomethane by means of either multiple separation steps with pressure gradients, or membrane contactors with concentration gradient as driving force. Among others, these membranes are usually made of polyimide, polysulfone and cellulose acetate polymeric materials (Angelidaki et al., 2018; Ballaguet et al., 2018; Ford, 2007; Kerber and Repke, 2016). Specific H_2S chemical desulfurization may be similarly feasible by using strong oxidation agents, such as H_2O_2, $KMnO_4$, Cl_2 and O_3 as currently done for wastewater treatment. However, possible methane oxidation frequently limits its application for biogas valorization (Bernard, 2013; Cadena and Peters, 1988; Lewkiewicz-Malysa et al., 2008). Biological H_2S removal has become increasingly popular with a wide range of techniques, e.g., continuous stirred-tank reactors, biofilters, and membrane contactors, which

use alkaline solvents to produce sulfide ions in liquid phase to thereafter biologically oxidize it to elemental sulfur. Frequent problems related to biomass accumulation and clogging, internal pH gradients, unwanted pressure drops and backmixing lead to decreased performance on these processes (Roman, 2016).

The use of a complete treatment unit, as well as integration of complementary units, is reported to be expensive and energy demanding for biogas treatment, due to its permanent changes of acid gases content, the singular presence of siloxanes, the low pressure (around 202.6 kPa) and the low flow rate (lower than 500 Nm^3/h) of raw biogas streams (Clément, 2016; Krischan et al., 2012; Vienna University of Technology, 2012).

Based on the described problem, a novel purification system has been developed for biogas applications. It allows eliminating the acid gases, siloxanes and NMVOCs up to the required emissions specifications, leading to a reduction of the total load factor of further separation equipment and thereafter energy savings. This system is based on the use of a superacid solvent mixture capable of performing a selective chemical absorption of the gas contaminants, by means of a bubble column reactor. The use of a superacid solvent has not been reported before for this type of applications.

This paper presents the process design considerations of the novel system: details on the solvent formulation, gas-liquid reaction mechanisms, transport properties specifications, equipment-dimensioning criteria and process simulation specifications. The newly proposed system was designed based on average composition values and flow rate of 500 Nm^3/h of a real biogas facility. The impurities content was set in dry basis equal to 400-1500 ppmv H_2S composition range, 30 % CO_2, 5 ppmv siloxanes, and 340 ppmv NMVOCs. A technical and energy-based feasibility study was also performed to the new process as compared to other commercialized technologies, i.e, the physical absorption with methanol, based on the Rectisol® process, and the chemical absorption with the monoethanolamine, MEA, aqueous solutions.

2. MATERIALS AND METHODS

2.1 Superacid solvent formulation

The proposed superacid solvent is a mixture of sulfuric acid ($H_2SO_{4(aq)}$, commercial grade, ≥95.0 wt. %) and acetic acid glacial ($CH_3COOH_{(l)}$, commercial grade, ≥99.8 vol. %). Scientific reports have been published describing the ability of this mixture to react with weak acids for which the H_2SO_4 was not capable by itself (Kotov et al., 1969; Olah et al., 2009).

Based on the acids mixture reaction properties, the solvent formulation for the biogas treatment has been established to a molar ratio of 9/1 for $H_2SO_{4(aq)}/CH_3COOH_{(l)}$ respectively. This mole ratio, named “Superacid 9/1”, allows taking advantage of the hydrodynamic solution properties and the absorption and reaction capabilities as it is described on this paper.

2.2 Process simulation environment

Overall process simulations have been carried out using Aspen Plus V8.6 software (Aspen Technology Inc., 2014). RadFrac module in Aspen Plus V8.6 was used for modeling the proposed bubble column reactor as well as other absorption columns aimed for comparisons. This module was set for a rate-based simulation conditions, which allowed controlling mass transfer and reaction conditions based on the height of the columns. The other process operation units were similarly simulated in Aspen Plus V8.6 software. Detailed engineering

specifications were evaluated for the bubble column reactor, for which hydrodynamic properties were established based on reported equations by means of a numeric model coded in VBA (Visual Basic for Applications) using the MS Excel software. These properties are presented hereafter.

3. THEORY AND CALCULATION

3.1 Process modeling and base case scenario

Figure 1 presents the process simulation diagram of a biogas purification unit for biomethane production, without considering any desulfurization unit. This type of process lay-out is particularly used in French biogas upgrading units, usually employing either activated carbon or NaOH scrubbing units, coupled to a PSA or a membrane separation unit for biomethane production (European Biogas Association (EBA), 2017). Biogas properties, compositions and overall operation conditions, considered on this analysis, belong to a real Landfill sourced biogas processing unit in France.

The process in Figure 1 departs with a raw biogas stream exposed to a flash unit (FLASH-1) for removing water along to condensates. A two stages compression system (C1 and C2) allows thereafter increasing the pressure from 101.32 kPa to around 861.30 kPa, followed by another flash unit (FLASH-2) separating any possible formed condensate. Given the high H_2S concentrations in raw biogas streams, the compressed biogas shall be additionally treated with activated carbon or any other desulfurization unit (not specified on the diagram of Figure 1) for removing the H_2S and partially the CO_2, producing a maximum SO_2 emissions concentration of 130 ppmv for the agricultural and rural sites. Following the process scheme in Figure 1, a Pressure Swing Absorption (PSA) or a unit produces a biomethane stream (purified biogas with methane content above 95 % and CO_2 below 4 %) and an off-gas stream, enriched in CO_2 and remaining H_2S. Finally, a furnace (FURNACE and CHIMNEY) leads to the formation of SO_2 and the combustion of remaining siloxanes and NMVOCs. Heat recovery can afterwards take place from stack gas emissions. The heat from the stack gas is recovered through a final heat exchanger (HX-4), leading to maintain the biogas digester to a temperature around 303 K.

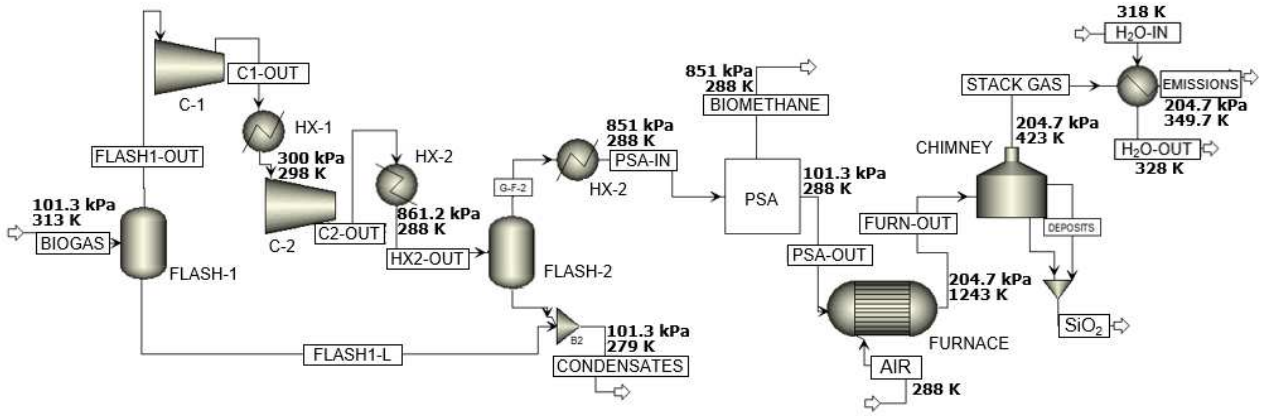

Figure 1. Biogas purification process – Scheme of the process simulation in Aspen Plus V8.6.

Overall technology assessment has been performed for a raw biogas stream of 500 Nm^3/h and for 3 different H_2S concentrations 400, 1000 and 1500 ppmv (dry basis, dew point at 268.15 K). Water and other compounds content varied proportionally to the water partial pressure in the gas. Table 2 presents the compositions of the base case scenario for purifying a raw biogas

stream of 400 ppmv H_2S (dry basis). Process simulations of the base scenario, with different H_2S content, were carried out considering the Electrolyte NRTL (ELECNRTL) with the Redlich-Kwong equation of state thermodynamic model for the liquid and gas phases properties, accounting for the gas compounds solubility through the different unitary operations and possible ions interaction. Silicates (SiO_2 aggregates) precipitation in the chimney was estimated after the combustion of siloxanes in the combustion chamber. The octamethylciclotetrasiloxane (D4) has been considered for representing the total siloxanes content in raw biogas. Based on the analyzed biogas sites, D4 showed to represent above 60 % of its total. Pentane, besides, has been chosen to represent the NMVOCs with a real participation of above 84 % of the total content of these compounds. The PSA unit was modeled for reaching 2 % CO_2 content in the produced biomethane and a maximum of 4 % CH_4 lost in the reject gas stream.

Flash units were simulated setting up duty (adiabatic) and pressure drop in a Flash module in the software. Compressors were set based on the discharge pressure with polytropic 75 % efficiency using the integrated ASME method. The modeled PSA technology unit was set using a user supplied subroutine, based on the reported adsorption capacity for the zeolite 5A as previously described. This unit operates normally by means of four adsorption columns producing biomethane with a pressure drop of 10-14 kPa and a residue/off-gas stream with a total pressure of 10-20 kPa absolute (Cherif, 2016; Deublein and Steinhauser, 2010). The rejected stream is then sent to feed the furnace at atmospheric pressure. This furnace was modeled using a Gibbs reactor and considering the oxidation of H_2S to SO_2, of hydrocarbons to CO_2, and of siloxanes D4 to SiO_2 with oxygen excess equal to 1 % at the outlet. Silicates precipitation was estimated at average chimney temperature of 423 K. Stack gas heat recovery is attained by a cross-flow heat exchanger leading to warm-up utility water from 318 to 328 K.

Table 2. Mass balance of the currently used process treatment for a biogas stream with 400 ppmv in H_2S (dry basis). Report obtained from process simulations in Aspen Plus V8.6.

	BIOGAS	FLASH1-OUT	PSA-IN	CONDENSATES	BIOMETHANE	PSA-OUT	AIR	SIO2	STACK GAS	H2O-IN	H2O-OUT	EMISSIONS
Temperature (K)	313.1	313.1	288.1	313.1	288.1	288.1	293.1	423.0	423.0	318.1	328.1	349.7
Pressure (kPa)	101.33	101.33	861.26	101.33	851.13	101.32	101.33	204.70	204.70	101.33	101.33	204.7
Vapor fraction	0.988	1	1	0.133	1	1	1	0	1	0	0	1
Flow rate (kmol/h)	22.321	21.332	21.218	1.103	8.734	12.484	6.892	<0.001	19.387	60	60	19.387
Molar concentration												
CH_4	0.407	0.425	0.428	897 ppmv	0.999	0.028	--	--	--	--	--	--
CO_2	0.287	0.293	0.295	0.131	0.001	0.500	300 ppmv	0.003	0.343	--	--	0.343
H_2S	383 ppmv	400 ppmv	402 ppmv	10 ppmv	--	683 ppmv	--	--	--	--	--	--
H_2O	0.044	0.006	867 ppmv	0.867	--	0.001	0.013	0.007	0.045	1	1	0.045
O_2	0.016	0.017	0.017	16 ppmv	--	0.029	0.207	115 ppm	0.052	--	--	0.052
N_2	0.239	0.250	0.250	179 ppmv	--	0.424	0.77	703 ppm	0.549	--	--	0.549
SO_2	--	--	--	--	--	--	--	18 ppm	440 ppmv	--	--	440 ppmv
Ar	0.007	0.007	0.007	6 ppmv		0.012	0.009	24 ppm	0.011			0.011
D4 (Siloxanes)	5 ppmv	45 ppb	46 ppb	109 ppmv	--	77 ppb	--	trace	10 ppb	--	--	10 ppb
SiO_2	--	--	--	--	--	--	--	0.99	trace	--	--	Trace
C_5 (NMVOCs)	338 ppmv	368 ppmv	402 ppmv	737 ppm	--	629 ppmv	--	--	--	--	--	--

The process illustrated in Figure 1 presents however some limitations, firstly, related to the frequent saturation of the currently used activated carbon in the desulfurization step, before the PSA, and the lack of a feasible technology for guaranteeing the mandatory SO_2

emissions levels. Secondly, poor H_2S purification unit leads to high H_2S concentrations within the process line and therefore to corrosion, environmental and security concerns for the personnel and facilities. Thirdly, the silicates precipitation in the combustion chamber and chimney are not necessarily controlled with the currently available processes; in consequence, the flame combustion temperature and the combustion efficiency are frequently reduced proportional to operating time (deposit formation). Lastly, the high SO_2 emission levels led to the reduction of the stack gas dew point (estimated to be around 318 K) and therefore the acid dew condensates formation in pipe lines and the final heat exchanger (Averill and Eldredge, 2012). The objective of the research presented on this paper is therefore to propose the use of a novel bubble column reactor with the Superacid 9/1 for the treatment of raw biogas streams, as shown in Figure 2. This reactor has been designed to replace activated carbon or any other desulfurization technology, after the compression units and before the PSA unit.

The bubble column reactor is presented on the right-hand side of Figure 2. The choice for this type of mass transfer equipment relied on the following criteria: it is recommended for simultaneous absorption and chemical reaction phenomena, especially if the global reaction velocity is higher than the mass transfer constant; it minimizes corrosion problems in internal parts, such as mixing impellers or packings; and it facilitates the solids handing (Majumder, 2016). These criteria are remarkably important for the required purification process that additionally stabilizes the H_2S in the gas producing solid elemental sulfur.

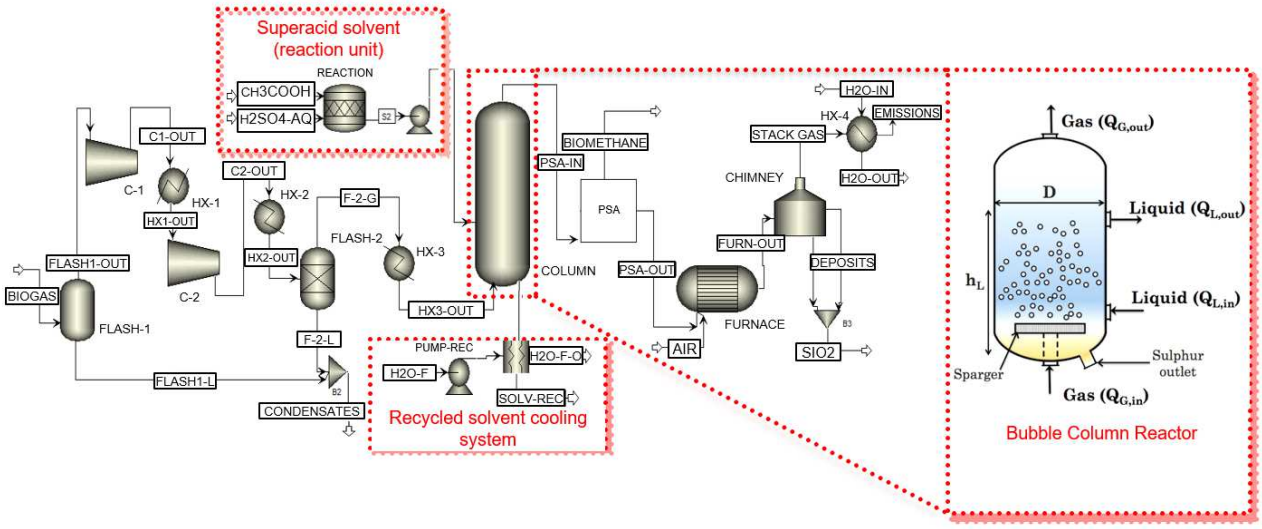

Figure 2. Biogas purification process including a bubble column reactor using the Superacid 9/1 for its purification – Process diagram in Aspen Plus V8.6.

3.2 Solvent chemical properties

Regarding the physical absorption properties of Superacid 9/1, each acid forming the superacid mixture exhibits interesting gas absorption capabilities. An extensive data review of the acid gases physical absorption, based on the solubility-based Henry's Law constant (H), is presented in Figure 3 for the H_2S, and in Figure 4 for the CO_2 (see Supplementary Material for data description). Different solvents have been used on the data analysis, based on the absorption mechanism: physical absorption, chemical absorption and hybrid absorption. Concerning the Henry constant (H) for the H_2S, shown in Figure 3, its value for the $CH_3COOH_{(l)}$ (99.8 vol.%) is equal to 36.044 $mol \cdot MPa^{-1}L^{-1}$ at 298 K and for the $H_2SO_{4\,(aq)}$ (95.0 wt.%) is equal to 2.266 $mol \cdot MPa^{-1}L^{-1}$ at the same temperature. Given the lack of

experimental data, these specific values were calculated using the Aspen Properties module considering the mentioned NRTL thermodynamic model. These values are consistently above the values shown by other widely used chemical solvents, especially for the acetic acid glacial. On the other hand, the CO_2 solubility Henry constant for the $CH_3COOH_{(l)}$ (99.8 vol.%) is equal to 1.857 $mol{\cdot}MPa^{-1}L^{-1}$ at 288 K and 0.320 $mol{\cdot}MPa^{-1}L^{-1}$ at 313 K for a 4 M aqueous solution ; whereas the same constant value for the CO_2 in $H_2SO_{4\,(aq)}$ (95.0 wt.%) is reported to be equal to 0.279 $mol{\cdot}MPa^{-1}L^{-1}$ at 298 K (Hansen, 2007; Rumpf et al., 1998). These values are similarly comparable to the ones reported by other commercial liquid solvents as shown in Figure 4.

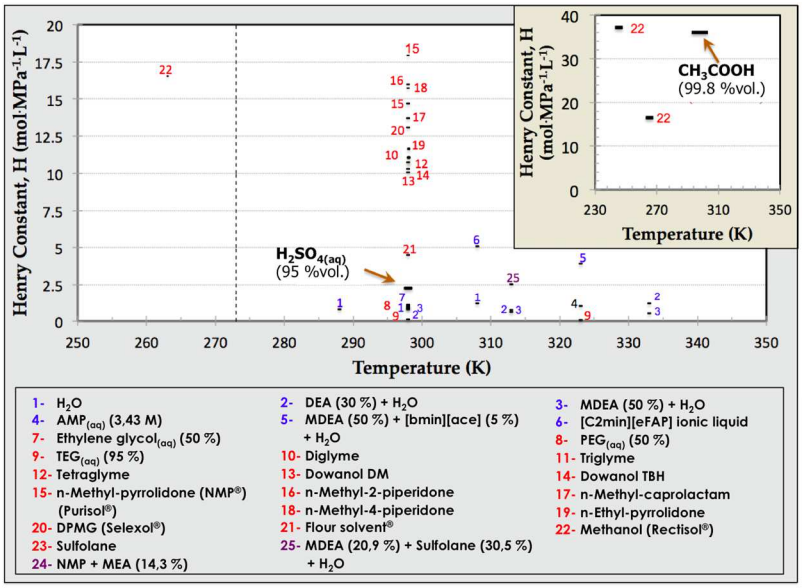

Figure 3. Solubility Henry constant for the H_2S absorption in different solvents: chemical absorption (in blue), physical absorption (in red) and hybrid absorption (in purple).

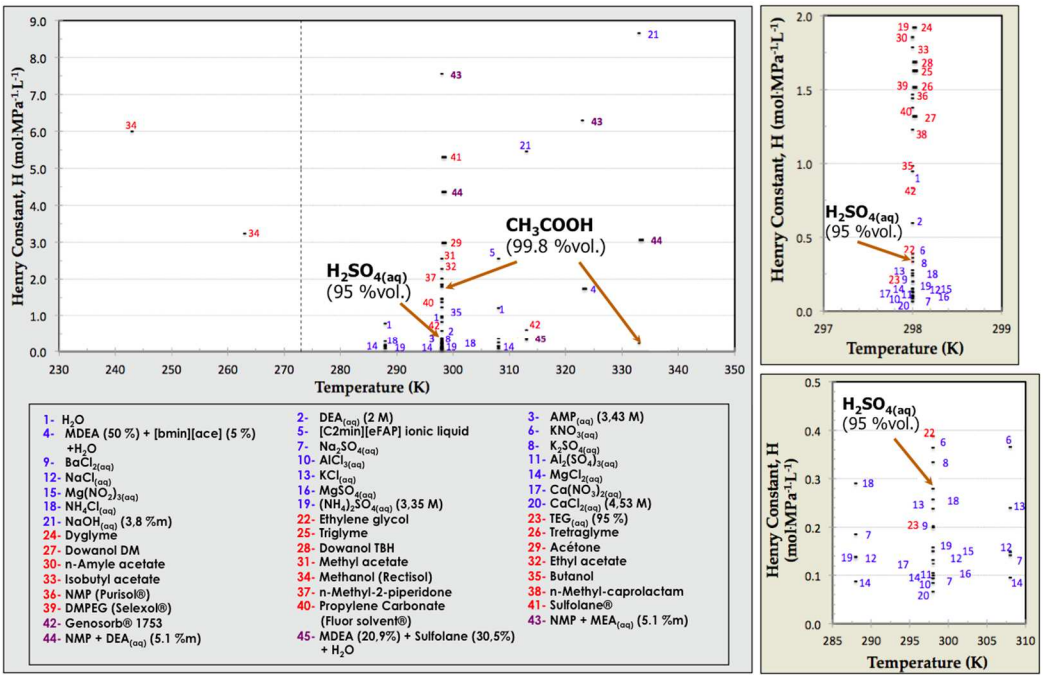

Figure 4. Solubility Henry constant for the CO_2 absorption in different solvents: chemical absorption (in blue), physical absorption (in red) and hybrid absorption (in purple).

As previously reported by the authors of this work, chemical solvents absorption capability is limited by reactivity and regeneration energy demands, whereas physical absorbents have proven to be limited by the gas partial pressures. In consequence, a combined effect (usually by means of a hybrid solvent) leading to combine the advantages of both systems results

attractive for the purification of gas streams (Charry-Prada et al., 2017). The proposed Superacid 9/1 allows considering both phenomena while eliminating the biogas impurities.

In terms of the superacid reactive properties, different reaction mechanisms are reported between the $H_2SO_{4(aq)}$ and the $CH_3COOH_{(l)}$, as a mixture by itself. These mechanisms were firstly reported by (Kotov et al., 1969), based on IR spectroscopy, conductometric and high-frequency titration analyses. They depend on the molar ratio between the two acids in the solution as a result of the chiefly by the charges on the atoms. The first mechanism is for an equimolar solution (1/1 for $H_2SO_{4(aq)}$/$CH_3COOH_{(l)}$ respectively), leading to the formation of the ionic species HSO_4^- and $CH_3C(OH)_2^+$ in a first step and thereafter the formation of cross-linked aggregates of molecules into a polymeric-based structure, which translates into a high viscosity solution. Secondly, an increase of the acids moles ratio above 3/2 for $H_2SO_{4(aq)}$/CH_3COOH respectively leads to the formation of superacid ions, avoiding the formation of cross-linked polymeric aggregates, and reducing the final solution viscosity. Finally, a higher content of the CH_3COOH compared to the $H_2SO_{4(aq)}$ in the solution does not promote any superacid ions species.

Considering the reports from (Kotov et al., 1969) indicate the formation of the superacid specie $CH_3C(OH)_2^+$ and the anion HSO_4^- (conjugate base) at the high constitutive acids ratio. The reaction shown in eq 1 is an approximation based on this mechanism, in which the cation $CH_3C(OH)_2^+$results from the nucleophilic protonation of the acetate anion, CH_3COO^- (Conant and Hall, 1927). The anions HSO_4^- and SO_4^{2-} are equally produced at the same molar ratio as given during the reported superacid species formation.

$$2CH_3COOH_{(l)} + 3H_2SO_{4(l)} + 6H_2O_{(l)} \rightarrow 2CH_3COO^-_{(aq)} + 2HSO^-_{4(aq)} + SO^{2-}_{4(aq)} + 6H_3O^+_{(aq)} \quad (1)$$

Relating to the eq 1, the anion HSO_4^- shall allow stabilizing the sulfuric acid for its further reaction with the H_2S from the gas stream. It was therefore directly implemented on the liquid stream feeding the bubble column reactor. The chemical conversion of CH_3COOH in eq 1 is estimated to 85 %, as shown in Table 3, based on the surface ratio between the IR spectra reported by (Kotov et al., 1969).

On the other hand, the reaction mechanism between the *in situ* formed superacid solvent and the raw biogas impurities, within the bubble column reactor, is proposed on this work as a result of diverse reported research works as hereafter described.

$$2H_2O_{(l)} \Leftrightarrow H_3O^+_{(aq)} + OH^-_{(aq)} \quad (2)$$

$$CO_{2(g)} + 2H_2O_{(l)} \rightleftharpoons H_3O^+_{(aq)} + HCO^-_{3(aq)} \quad (3)$$

$$HCO^-_{3(aq)} + H_2O_{(l)} \rightleftharpoons H_3O^+_{(aq)} + CO^{2-}_{3(aq)} \quad (4)$$

$$H_2S_{(g)} + H_2O_{(l)} \rightleftharpoons HS^-_{(aq)} + H_3O^+_{(aq)} \quad (5)$$

$$HS^-_{(aq)} + H_2O_{(l)} \rightleftharpoons S^-_{(aq)} + H_3O^+_{(aq)} \quad (6)$$

$$H_2SO_{4(l)} + H_2O_{(l)} \rightleftharpoons HSO^-_{4(aq)} + H_3O^+_{(aq)} \quad (7)$$

$$HSO^-_{4(aq)} + H_2O_{(l)} \rightleftharpoons SO^{2-}_{4(aq)} + H_3O^+_{(aq)} \quad (8)$$

$$CH_3COOH_{(l)} + H_2O_{(l)} \rightleftharpoons CH_3COO^-_{(aq)} + H_3O^+_{(aq)} \quad (9)$$

$$CO_{2(aq)} + OH^-_{(aq)} \rightarrow HCO^-_{3(aq)} \quad (10)$$

$$HCO^-_{3(aq)} \rightarrow CO_{2(aq)} + OH^-_{(aq)} \quad (11)$$

$$H_2S_{(g)} + H_2SO_{4(l)} \rightarrow S_{(s)} + SO_{2(aq)} + 2H_2O_{(l)} \quad (12)$$

$$2H_2S_{(aq)} + SO_{2(aq)} \rightarrow 3S_{(s)} + 2H_2O_{(l)} \quad (13)$$

$$2H_2S_{(aq)} + O_{2(aq)} \rightarrow 2S_{(aq)} + 2H_2O_{(l)} \quad (14)$$

$$C_8H_{24}O_4Si_{4(g)} + 12H_2SO_{4(l)} \rightarrow 4(CH_3)_2Si(HSO_4)_{2(l)} + 4HSO^-_{4(aq)} + 4H_3O^+_{(aq)} \quad (15)$$

First, reactions from eq 2 to eq 9 describe the species dissolution, as water is a component in the gas and liquid phases. For these reactions, equilibrium constants are calculated by Gibbs free energy minimization, as possible with the Aspen Plus simulation software.

Second, forward reactions in eq 10 and eq 11 correspond to the CO_2 interactions with the system ionic species in the liquid phase; whereas reactions, eq 12 and eq 13, describe the chemical reactions proposed by (Wang et al., 2002b, 2002a; Zhang et al., 2000) for the H_2S reduction using concentrated sulfuric acid solutions. Experimental work from the mentioned authors led to establishing their optimized reaction parameters shown in Table 3, considering the reactions at the liquid surface interface, for a reaction temperature below 333 K and pure H_2S gas (Wang et al., 2002b, 2002a; Zhang et al., 2000). These authors however emphasized the need for high H_2SO_4 solvent concentration, above 80 vol. %, in order to allow the reaction conversion to elemental sulfur. In consequence, the solvent formulation for the biogas treatment has been established considering an excess of $H_2SO_{4(aq)}$ and therefore to molar ratio of 9/1 for $H_2SO_{4(aq)}/CH_3COOH_{(l)}$ respectively (Superacid 9/1). Reaction rate expressions for these reactions, as well as its specific Arrhenius constants, are presented in Table 3.

Third, the eq 14, represents the generalized reaction between H_2S and solubilized oxygen (O_2). This reaction is usually induced by the presence of microorganisms at pH values around 7 in sewers and aquifers, but it is also naturally produced by chemical reactions in acid environments with a pH below 4 (Deublein and Steinhauser, 2010; Marriott et al., 2016; Nielsen et al., 2006).. This last condition is in agreement with the reaction conditions with the superacid solution. Secondary reactions have been similarly reported between the H_2S and the O_2 leading to the formation of thiosulfites such as the SO_3^{2-} and the $S_2O_3^{2-}$ (Marriott et al., 2016; Nielsen et al., 2006; Siang et al., 2017), other species from the self-hydration of H_2SO_4, such as the $S_2O_7^{2-}$ and the $HS_2O_7^-$ (Borisov et al., 1971). These sulfur ionic species are however easily decomposed in acid environments, especially in presence of H_2SO_4 (Zhang et al., 2000). Significant oxygen content in biogas streams may additionally result from badly isolated landfills. The overall reaction conversion is presented in Table 3.

Table 3. Kinetic parameters (Arrhenius law) and conversion values of forward reactions between the raw biogas and the Superacid 9/1

Reaction	Reaction rate, r_i ($mol \cdot m^{-3} \cdot s^{-1}$)	Activation energy, Ea ($kJ \cdot mol^{-1}$)	Pre-exponential factor, A_0	Conversion ($mol \cdot mol^{-1}$)	Reference
(1)	---	---	---	0.85	(Kotov et al., 1969)
(10)	$r_{CO_2} = A_0\, e^{(-E_a/RT)}\, C_{CO_2} C_{OH^-}$	55.434	4.32×10^{13} $m^3 mol^{-1} s^{-1}$ (*)	---	(Aspen Technology Inc., 2013)
(11)	$r_{HCO_3^-} = A_0\, e^{(-E_a/RT)}\, C_{HCO_3^-}$	123.256	2.38×10^{17} s^{-1}	---	(Aspen Technology Inc., 2013)
(12)	$r_{H_2S} = A_0\, e^{(-E_a/RT)}\, C_{H_2S}$	$-178 + 2.23\, C_{AS}$	7.99×10^{-6} s^{-1}	---	(Wang et al., 2002a)
(13)	$r_{H_2S} = A_0\, e^{(-E_a/RT)}\, C_{H_2S} C_{SO_2}$	59.02	526.33 $m^3 mol^{-1} s^{-1}$ (**)	---	(Wang et al., 2002b)
(14)	---	---	---	0.415 (83 g S/g O_2)	(Nielsen et al., 2006)
(15)	---	---	---	0.70	(Ruiling et al., 2017)

C_{AS} : $H_2SO_{4(aq)}$ concentration (wt. %)
(*) Corresponding value for the operating conditions: $H_2SO_{4(aq)}$ concentration, pressure and temperature
(**) Value assuming 1 mole/22.4 L for the gas

The elemental sulfur precipitation was understood to occur by the formation of the cyclic allotrope orthorhombic structure ($\alpha - S_8$), which is the stable form at room pressure and temperature and up to 341 K, meaning that $S^0 = 1/8\, S_8$ (Crapanzano, 2008).

Finally, resulting from the simplification done on this work about considering D4 to represent the siloxanes content in the biogas, eq 15 exemplifies the chemical degradation of siloxanes by means of concentrated sulfuric acid solutions. Related process yields have been previously reported by (Ricaurte Ortega, 2009; Ruiling et al., 2017; Soreanu et al., 2011) and the chemical conversion for the proposed process is tabulated in Table 3. The reaction in eq 15 results from the Si-O bond cleavage of the cyclic siloxanes by the sulfuric acid, followed by a nucleophilic substitution. This mechanism is reported as validated by cryoscopic and conductivity-based analyses, leading to the formation of the non-electrolyte $(CH_3)_2Si(HSO_4)_2$ specie (Borisov et al., 1971; Cypryk and Apeloig, 2002; Flowers et al., 1963). For modeling purpose of this work, the $(CH_3)_2Si(HSO_4)_2$ physico-chemical properties have been estimated using the online molecular software ChemRTP® (ChemEssen-Inc., 2017), in which the calculation methods are based on quantitative structure-activity relationship models (QSAR models) from the molecular extractions.

3.3 Equipment properties and design

Process simulations through Aspen Plus V8.6 software allow determining feasible operational conditions, as well as heat and mass balance calculations. In terms of the design specifications of the proposed bubble column reactor, it was however necessary to confirm the optimal conditions for the gas dispersion in the liquid phase (bubble-scale properties), the proper equipment operation and fluids velocity (reactor-scale properties), and the good performance of the reactor face to process instabilities (industrial-scale properties). Analysis of these properties led to optimal designs and mass transfer enhancement between the phases (Besagni et al., 2018; Fair et al., 1999). For the RadFrac module in Aspen Plus, besides the used ELECNRTL thermodynamic model, simulations considered 7 packing theoretical stages, and the packing parameters corresponding to a plastic mellapak Sulzer's supplier with a parameterized interfacial area a_i~20 m^2/m^3, corresponding to bubbling columns as discussed later on this article. The rate-based calculation considered a mixed flow model and reactive film resistances for the gas and liquid phases. Software existing mass transfer coefficient method from (Bravo and Rocha, 1985) were used as considering full wetting and interchannel flow as it may occur in a bubbling regime.

On the other hand, the equations considered for evaluating the dispersion conditions and therefore for the hydrodynamic stability of the bubble column reactor were set in a coupled VBA routine integrating the equations tabulated in Table 4. This equipment has been conceived as vertical column with a gas and a liquid co-current flow from the bottom to the top of the vessel, with a discharge for the produced elemental sulfur (solids) at the bottom, and with a gas sparger (Figure 2 right-hand side image). Ideally, the internal flow shall be controlled to a "bubbly flow" regime, which renders the gas dispersion as bubbles show tendency to concentrate towards the center of the pipe without axial or radial oscillations. This regime avoids possible liquid backmixing issues, as reported by several authors (Besagni et al., 2018; Majumder, 2016; Shah et al., 1978; Tilton, 2008). Bubbly flow regime is principally established based on bubble-scale properties, i.e., a low gas-liquid volume ratio at the inlet of the reactor ($Q_G/Q_L < 2$), low gas and superficial liquid velocities ($U_G < 0.06$ m/s and $U_L < 0.2$ m/s), and small sparger pore diameters ($d_0 < 0.015$ m) (Besagni et al., 2018; Tilton, 2008;

Wu and Al-Dahhan, 2001). Eq 16 allows determining an average U_G value in the reactor, based on the overall mass balance; whereas eq 17 and eq 18 allow estimating a liquid phase velocity based on the equipment and fluids properties. All the designed cases of this work considered a $d_0 = 0.003$ m.

Table 4. Principal hydrodynamic properties considered for designing the bubble column reactor

Parameter	Correlation	Range of parameters in Bubbly flow	Reference
Bubble-scale properties			
$\mathbf{U_G}$	$U_{G,avg} = \left(\frac{F_{g,avg}}{a}\right)\left(\frac{Mw_L}{\rho_{g,avg}}\right)\left(\frac{Q_G}{Q_G+Q_L}\right)$ (16)	For D>0.15 m, U_G<0.04 -0.06 m/s	(Besagni et al., 2018; Majumder, 2016)
$\mathbf{U_L}$	Zehner (1986): $U_L = 0.737\left(U_g\, D\right)^{1/3}$ (17) Riquarts (1981): $U_L = 0.21(g\, D)^{1/2}\left(U_G{}^3\, \rho_L/g\, \mu_L\right)^{1/3}$ (18)	For $Q_G/Q_L < 2$, $U_L < 0.061\ m/s$	(Tilton, 2008; Wu and Al-Dahhan, 2001)
$\mathbf{d_b}$	Moo-Young (1981): $d_b = 0.19\, d_o^{0.48}\, Re_o^{0.32}$ (19) Wilkinson et al. (1994): $d_b = \left[8.8\left(\frac{\sigma_L}{g\,\rho_L}\right)\left(\frac{U_G\,\mu_L}{\sigma_L}\right)^{-0.04}\left(\frac{\sigma_L{}^3\rho_L}{g\,\mu_L{}^4}\right)^{-0.12}\left(\frac{\rho_L}{\rho_G}\right)^{0.22}\right]^{1/2}$ (20)	For U_G<0.04 -0.06 m/s d_b < 0.008 m.	(Kantarci et al., 2005; Nedeltchev, 2017; Sarrafi, 1999)
$\mathbf{AR_b}$	$AR_b = \frac{1}{1+0.0553\ Eo^{0,266}}$ (21) where $Eo = \frac{g\,\rho_L\, d_b{}^2}{\sigma_L}$		(Besagni et al., 2018)
$\mathbf{U_b}$	Jamialahmadi et al. (1991): $U_b = \frac{U_{bs}U_{bw}}{\sqrt{U_{bs}{}^2+U_{bw}{}^2}}$ (22) where, $U_{bs} = \frac{1}{18}\frac{\rho_L-\rho_G}{\mu_L} g d_b{}^2 \frac{3\mu_L+3\mu_G}{2\mu_L+3\mu_G}$ and $U_{bw} = \sqrt{\frac{2\,\sigma_L}{d_b(\rho_L-\rho_G)}+\frac{g\,d_b}{2}}$ D.Darmana et al. (2005): $U_b = \left(\frac{4(\rho_L-\rho_G)\,\sigma_L\, g}{\rho_L{}^2}\right)^{1/4}$ (23)	For D>0.15 m and d_b < 0.005 m, $U_b < 0.2\ m/s$	(Darmana et al., 2005; Jamialahmadi and Muller-Steinhagen, 1990; Sarrafi, 1999)
$\mathbf{C_{vm}}$	Lance & Bataille (1991) : $C_{vm} = \frac{1}{2}\left(1 + 2.7\frac{Q_G}{Q_G+Q_L}\right)$ (24)	Bubbles in "Bubbly flow" are: C_{vm}~0.15 (spherical) $C_{vm} = 0.70 - 1.52$ (ellipsoid)	(Kolev, 2005; Lopez de Bertodano et al., 1994)
Reactor-scale properties			
$\boldsymbol{\mathcal{E}_G}$	Joshi & Sharma (1979): $\mathcal{E}_G = \frac{U_G}{0.3+2\,U_G}$ (25) Hughmark (1967): $\mathcal{E}_G = \frac{1}{2+\left(\frac{0.35}{U_G}\right)\left(\frac{\rho_L\,\sigma_L}{72}\right)^{1/3}}$ (26) Hikita et al. (1980): $\mathcal{E}_G = 0.627\ I_f \left(\frac{\mu_G\,\mu_L}{\sigma_L}\right)^{0.578}\left(\frac{\mu_L^4\, g}{\rho_L\,\sigma_L{}^3}\right)^{-0.131}\left(\frac{\rho_G}{\rho_L}\right)^{0.062}\left(\frac{\mu_G}{\mu_L}\right)^{0.107}$ (27) where, $I_f = \begin{cases} 10^{0.0414\,I} & \text{... if } \left(0 < I < 1\ {}^{g}/_{L}\right) \\ 1.1 & \text{... if } \left(I > 1\ {}^{g}/_{L}\right) \end{cases}$	$\mathcal{E}_G < 0.15$, *For Hughmark (1967)*: $U_G = 0.4 - 45$ cm/s and $D > 0.01\ m$ *For Joshi et Sharma (1979)*: Bubbly flow *For Hikita et al. (1980):* $U_G < 0.1$ m/s	(Besagni et al., 2018; Hikita et al., 1980; Sarrafi, 1999)
$\mathbf{a_i}$	Akita & Yoshida (1974) : $a_i = \frac{1}{3\,D}\left(\frac{g\,D^2\rho_L}{\sigma_L}\right)^{0.5}\left(\frac{g\,D^3\rho_L{}^2}{\mu_L{}^2}\right)^{0.1}\mathcal{E}_G{}^{1.13}$ (28)	For $\mathcal{E}_G < 0.14$, a_i~20 ${}^{m^2}/_{m^3}$	(Besagni et al., 2018; J. C. Middleton et al., 1997)
$\mathbf{K_L}$	Shah et al. (1982): $K_L a_i = 0.467\ U_G{}^{0.82}$ (29) Kang et al. (1999): $K_L a_i = 10^{-3.08}\, D\left(\frac{DU_G\rho_G}{\mu_L}\right)^{0.254}$ (30)	For $U_G < 0.15$, $K_L a_i = 0.005 - 0.02\ s^{-1}$	(Besagni et al., 2018; J. C. Middleton et al., 1997; Shah et al., 1982)
$\boldsymbol{\phi_c}$	$\phi_c = \frac{\text{Mixing time}}{\text{Mass transfer time}} = \frac{h_L{}^2/(1-\mathcal{E}_G)\,E_{DL}}{1/K_L a_i}$ (31)		(Deckwer and Schumpe, 1993)
$\mathbf{tr_G}$	$tr_G = \frac{h_L\,\mathcal{E}_G}{(1-\mathcal{E}_G)\,U_G}$ (32)		(Kirk et al., 2000)
Industrial-scale properties and dimensionless numbers			
$\mathbf{d_b{}^{max}}$	Ishii & Kojasoy (1993): $d_b{}^{max} = 40\sqrt{\frac{\sigma_L}{g(\rho_L-\rho_G)}}$ (33)	$(d_b \le d_b{}^{max})$	(Besagni et al., 2018)
$\mathbf{D_H{}^*}$	Rayleigh-Taylor Instability: $D_H{}^* = \frac{D}{\sqrt{\sigma_L/g(\rho_L-\rho_G)}}$ (34)	$(D_H{}^* < 52\ h_L)$	(Besagni et al., 2018)
$\mathbf{AR_c}$	$AR_c = \left(\frac{h_L}{D}\right)(1-\mathcal{E}_G)$ (35)	$(AR_c < 5)$	(Besagni et al., 2018)
$\mathbf{f_l}$	Joshi et al. (2001): $f_l = 1 - \frac{\left[B_1\left({}^{B_6}/_{B_5}\right) - {}^{B_2}/_2\right]^2}{B_1(B_4-B_3)+{}^{B_2{}^2}/_4}$ (36) where, $B_1 = \frac{\rho_G}{\rho_L} + \left(\frac{1+Cv}{1-\mathcal{E}_G}\right) - 1$; $B_2 = 2\left(\frac{\rho_G}{\rho_L} + C_{vm}\right)\left(\frac{U_{slg}+U_G}{\mathcal{E}_G}\right) + 2\left(\frac{\mathcal{E}_G}{1-\mathcal{E}_G}\right)C_{vm}\left(\frac{U_G}{1-\mathcal{E}_G}\right)$; $B_3 = \left(\frac{\rho_G}{\rho_L} + C_{vm}\right)\left(\frac{U_{slg}+U_G}{\mathcal{E}_G}\right)^2 + \left(\frac{\mathcal{E}_G}{1-\mathcal{E}_G}\right)C_{vm}\left(\frac{U_G}{1-\mathcal{E}_G}\right)^2$; $B_4 = \frac{\beta_0}{\rho_L}\left(\frac{E_{DL}}{1-\mathcal{E}_G} + \frac{E_{DG}}{\mathcal{E}_G}\right)$; $B_5 = \frac{\beta_0}{\rho_L}\left(\frac{1}{1-\mathcal{E}_G} + \frac{1}{\mathcal{E}_G}\right)$ $B_6 = \frac{\beta_0}{\rho_L}\left(\frac{U_{slg}+U_G}{\mathcal{E}_G} + \frac{U_G}{1-\mathcal{E}_G}\right) + \frac{\beta_0}{\rho_L}U_{slg} + g\frac{(\rho_G-\rho_L)}{\rho_L}$; $\beta_0 = \frac{(\rho_G-\rho_L)\mathcal{E}_G\, g}{U_{slg}}$	$f_l < 0$ Unstable $f_l > 0$ Stable	(Besagni et al., 2018; Fair et al., 1999; Joshi et al., 2001)
$\mathbf{E_{DG}}$	$E_{DG} = 56.4\ D^{1.33}\left(\frac{U_G}{\mathcal{E}_G}\right)^{3.56}$ (37)	To avoid liquid backmixing, $E_{DG} \gg E_{DL}$	(Fair et al., 1999; Shah et al., 1978)
$\mathbf{E_{DL}}$	$E_{DL} = 0.35\ U_G\, D\left(\frac{g\,D}{U_G{}^2}\right)^{1/3}$ (38) Hikita & Kikukawa (1974): $E_{DL} = (0.114 + 0.523\ U_G{}^{0.77})\ D^{1.25}\left(\frac{1}{\mu_L}\right)^{0.12}$ (39)		
$\mathbf{Pe_G}$	$Pe_G = \frac{h_L\,U_G}{\mathcal{E}_G\,E_{DG}}$ (40)	$(Pe_L < Pe_G)$	

Pe_L	$Pe_L = \frac{h_L U_L}{(1-\varepsilon_G) E_{DL}}$	(41)	$Pe_G = 0$: Liquid backmixing $Pe_G \to \infty$: Full axial flow	(Deckwer, 1985; Shah et al., 1978)
Fr_G	$Fr_G = \frac{U_G^2}{g D}$	(42)		(Wu and Al-Dahhan, 2001)
Fr_L	$Fr_L = \frac{U_L}{\sqrt{g(\rho_L - \rho_G) D/\rho_L}}$	(43)	$\left[Fr_L \leq \left(\frac{h_{L,min}}{D}\right)^2\right]$ (44)	(Tilton, 2008)
Bd	$Bd = \frac{\rho_L g d_b^2}{4\sigma_L}$	(45)	Stability at Bd < 0.2 and We < 0.4 for aqueous solutions of alcohols and electrolytes	(Shah et al., 1982)
We	$We = \frac{\rho_L U_b^2 d_b^2}{2\sigma_L}$	(46)		

Calculation of the mean bubbles diameter (d_b), either by eq 19 or eq 20, provides information regarding the shape of the bubbles and their stability in a bubbly regime: normally, $d_b < 0.2$ mm is characteristic for rigid mobile spheres, $0.2\ mm < d_b < 2$ mm lead to spheroids or ellipsoidal bubbles, and $d_b > 1$ cm means mobile spherical caps. Special attention is given to eq 20, from *Wilkinson et al. (1994)*, which is reported to be the most accurate formulation to estimate d_b (Besagni et al., 2018; Nedeltchev, 2017). Alternatively, bubble aspect ratio (AR_b) calculation, eq 21, provide indication of the spheroids formation for $AR_b \ll 1$ (Besagni et al., 2018). Calculation of the rise velocity of non-spherical bubbles (U_b), eq 22 or eq 23, allows denoting a bubbly regime for $d_b < 0.008$ m, based on several experimental data and analyses reported by (Jamialahmadi and Muller-Steinhagen, 1990). Finally, the definition of a virtual mass coefficient (C_{vm}), eq 24, is important for bubble-based dispersion systems, representing the inertia of the bubble-induced fluid flow (Kolev, 2005; Lopez de Bertodano et al., 1994). This parameter is used to determine the column stability providing information about the mean bubbles shape as described in Table 4.

Concerning the reactor-scale properties, the gas holdup (ε_G) is the controlling parameter for the gas-in-liquid dispersions. ε_G represents the volumetric fraction of the bubbles in the liquid phase (Fair et al., 1999; Kantarci et al., 2005). Different equations are available in the scientific literature for ε_G, three of the most widely reported are presented in Table 4: eq 25 from *Joshi & Sharma (1979)* based only on the U_G, eq 26 from *Hughmark (1967)* based on gas and liquid properties, and eq 27 from *Hikita et al. (1980)* as the only one considering effect of ionic species in the liquid phase. Eq 27 has reported up to 4 % higher precision than the other equations used to describe the gas holdup, as reported by (Besagni et al., 2018; Sarrafi, 1999) based on experimental data. Based on these, values of $\varepsilon_G \leq 15$ % are needed, independently of the pore size of the sparger, in order to establish a homogeneous bubbly regime within the reactor. Adequate gas holdup controls the liquid circulation and thus the interphase contact between the gas and the liquid solvent (a_i), described by eq 28. (J. C. Middleton et al., 1997) have proposed a nominal value of $a_i \sim 20\ m^2/m^3$ for the bubbling columns, based on experimental data analyses, therefore applicable for the bubble column reactor of this study. Equally related to the mass transfer at the interface level, the liquid mass transfer coefficient (K_L), defined by eq 29 and/or eq 30, certainly limits the overall reaction rate at the bulk liquid phase. (J. C. Middleton et al., 1997) have similarly proposed a nominal range of $K_L a_i = 0.005 - 0.02\ s^{-1}$ for bubbling columns based on experimental data analyses.

Studies reported by (Kirk et al., 2000) suggest that up to 15 wt. % of suspended solids in a gas-in-liquid dispersion do not affect the $K_L a_i$ values and therefore the overall mass transfer phenomenon. In consequence, elemental sulfur precipitation, as a result of the reaction properties of this work, has been considered to have a negligible effect on the hydrodynamic modeling.

On the reactor-scale properties, two other characteristic parameters appear to describe the ratio between the mixing time and the mass transfer time (ϕ_c), eq 31, and the gas residence time on a bubble column (tr_G), eq 32. The ϕ_c denotes the prevalence of one phenomenon over

the other within the gas dispersion process; whereas the tr_G is important to define the proper modeling conditions of the bubble column reactor. In fact, since a tr_G value is an equipment simulation input for the RadFrac module on Aspen Plus V8.6, a numerical iteration was performed by reducing the error between two consecutive calculations of tr_G to values lower than 3 %. The initial iteration condition was determined assuming $tr_G \sim 1/K_L a_i \sim 1/0.0125\ s$

Once the reactor-scale properties were established, industrial-scale stability was to be confirmed by means of the equations in Table 4. These instability criteria refer to the bubbles and the gas-to-liquid phase perturbations, which render a disorganized and chaotic bubbling and a limited mass transfer between the phases due to radial dispersions (Besagni et al., 2018). Instable regime results led to modifying design parameters, principally the reactor's diameter or the gas-to-liquid volume ratio, until reaching values relying on the needed design specifications. The first stability criterion corresponds to the maximum bubble diameter (d_b^{max}) established by *Ishii et Kojasoy (1993)* and based on the Kelvin-Helmholtz instability, eq 33. This instability defines the possible bubbles break-up condition due to velocity gradients around its surface leading to shear stresses causing pressure fluctuations alongside the interface and bubble–eddy collisions (Besagni et al., 2018). Bubbly regime inside the bubble column reactor demands a $d_b < d_b^{max}$ for all conditions. The second criterion relates the difficulty to control the gas and liquid phase velocities in industrial-scale columns with the phenomenon described as the Taylor–Rayleigh instability. This instability arises whenever a lighter fluid is accelerated into a heavier fluid as a result of the density difference between the liquid and the gas phases avoiding the bubbles formation through the column height. In order to limit this phenomenon and homogenize the bubbly regime, a hydraulic diameter value of $D_H^* < 52h_L$ has been proposed for industrial bubbly columns, as described by eq 34 (Besagni et al., 2018). Similarly, (Besagni et al., 2018) proposed a critical bubble-column aspect ratio (AR_c) as defined in eq 35. Experimental results from these authors in discontinuous and co-current flows in bubble columns suggests that values of $AR_c > 5$ allow radial dispersion occurrence; in consequence, the bubbles size distribution becomes heterogeneous and therefore may coalescence before reaching the liquid surface. Finally, a generalized hydrodynamic stability factor (f_l), proposed by (Joshi et al., 2001), is described by eq 36, for which stability may be guarantee for $f_l > 0$. This stability model was established using a one-dimensional model for multiphase systems based on linear stability theory and considering possible system perturbations on the diffusivity, the mass transfer and the Reynolds stress accounting for the velocity variation during the fluids movement. f_l coefficient was defined in terms of the gas-phase and liquid-phase axial dispersion coefficients. These parameters are defined by eq 37 for the gas-phase axial dispersion coefficient (E_{DG}) and, by eq 38 and eq 39 for the liquid-phase axial dispersion coefficient (E_{DL}). Reports from (Fair et al., 1999) insist on the need of higher values of E_{DG} than E_{DL} in order to avoid liquid axial backmixing issues.

Representative dimensionless numbers evaluated on the bubble column reactor are also tabulated on Table 4. Concerning these parameters, theoretical studies from (Fair et al., 1999) have established the Peclet number of the gas-phase (Pe_G), eq 40, and the Peclet of the liquid-phase (Pe_L), eq 41 for bubble columns. $Pe_G > Pe_L$ values are nevertheless recommended in bubble systems for limiting the effect of the axial dispersions at industrial-scale while reducing the risk of liquid backmixing. Liquid backmixing phenomenon normally reduces from top to bottom of the column, as suggested by experimental results from (Deckwer, 1985). On the other hand, the definition of Froude number of the liquid-phase (Fr_L), eq 42, and Froude number of the gas-phase (Fr_G), eq 43, were used by (Shah et al., 1978) in order to establish the minimum liquid height to avoid a physical phase separation within the column due to bubbles coalescence

($h_{L,min}$), eq 44. Finally, the relationship between de Bond number (Bd), eq 45, and the Webber number, eq 46, has been reported by (Tilton, 2008) by means of the so-called Berghmans diagram. This diagram, based on experimental observations, reports the stability limits of Bd and We numbers for bubble systems with ionic species. These limits refer to the bubbles break-up conditions and they are presented in Table 4 for the studied bubble column reactor.

Industrial implementation of the proposed bubble column reactor, using the superacid solvent, requires special attention regarding the structural material of the equipment. Preliminary materials scouting shows that stainless steel alloys used for the phosphoric acid industry may suit and resist corrosion. Their content of molybdenum and nickel shall be high. Besides, several epoxy resins are under development for sulfuric acid reservoirs.

3.4 Comparison with other purification technologies

A technical comparison was carried out between the proposed bubble column reactor and two other feasible biogas purification technologies: the physical absorption with methanol and the chemical absorption with a 17 wt. % aqueous solution of the alkanolamine MEA. Energy demand analyses for all the processes were carried out considering a Pinch number equal to 5 for the modeled heat exchangers and a coefficient of performance (COP) was used to equate to lower operating energy demands and costs. The COP sets the efficiency between the available thermal energy and the energy power requirement (Smith et al., 2005). In overall, a COP of 5 was considered for the cooling systems using water utility (temperature above 273 K); whereas a thermal efficiency of Carnot equal to 45 % was set to determine the thermal efficiency leading to a refrigeration to temperatures below 273 K.

Physical absorption with methanol results attractive for biogas purification, and therefore comparable the proposed bubble column reactor, because of the following reasons:

- Methanol exhibits a high absorption capability for the acid gases (CO_2 and H_2S) as represented in terms of the solubility Henry constant. The H_2S related Henry constant is equal to 37.13 $mol{\cdot}MPa^{-1}L^{-1}$ as shown in Figure 3; whereas the CO_2 related Henry constant is equal to 6.00 $mol{\cdot}MPa^{-1}L^{-1}$, both at 240 K, as shown in Figure 4. This Henry constant reduces as the temperature is increased.
- Methanol has proven industrial-scale absorption capabilities to reduce acid gases in petrochemical and carbon-gasification processes. It allows producing a purified gas with at least CO_2 content below 0.4 % and H_2S content below 0.1 ppmv, at temperatures around 199-213 K and pressures between 2.73-7.96 MPa abs (Kohl and Nielsen, 1997).
- Methanol is additionally suggested for the NMVOCs and siloxanes separation from gas streams with a removal efficiency between 95-99 % in function of the operation temperature (Ruiling et al., 2017).
- The available high-pressure gas stream leaving the compression system and entering the PSA (in agreement with the process from, Figure 2), at around 861.26 kPa (see Table 2), justifies the use of a purification unit based on physical absorption by reducing further compression energy need.

It is worth mentioning that using methanol as a solvent may however result in safety concerns mostly during its storage, given its flammability, with an auto-ignition temperature of 658.15 K (Methanol Institute (MI), 2016). The use of this solvent is however well-known and stablished ; entire processes, such as Rectisol® are based on its use for gas treatment (Kohl and Nielsen, 1997).

The conceived methanol-based purification unit results from a simplification of the existing Rectisol® process, using a single absorption column and a refrigeration unit for conditioning the solvent before it can be recycled. The simulation process diagram is presented in Figure 5 a. Operating conditions of this process were optimized by maximizing the acid gas elimination and by minimizing the solvent loss within the gas phase. This process requires in overall four new sets of operation units as compared to the base case scenario shown in Figure 1. First, the absorption unit simulated as a packed column by using the rate-based RadFrac module in Aspen Plus V8.6. This column may operate with 7 theoretical stages, in counter-current flow with the liquid feed from the top and the gas feed from the bottom of the column, imposing a film resistance between the phases given by the Henry constant condition in the simulation module. Second, a compressor and a heat exchanger used to set a gas feed to the column at 2735.8 kPa and 278.15 K. These conditions represent the minimal operating pressure of the first stage for an industrial Rectisol® process (Kohl and Nielsen, 1997) and the minimal temperature required to avoid possible dew pointing and solvent evaporation. Third, a pump followed by a heat exchanger, assuring a liquid feed pressure to the column equal to 2735.8 kPa and 205 K. This temperature has been optimized in order to attain the highest H_2S separation efficiency. Finally, a refrigeration system needed for conditioning the acid gas-enriched solvent leaving the bottom of the column, to be later adiabatically expanded for desorbing the separated acid gases. The lean solvent is then sent through a cross heat exchanger to cool it down before being recycled to the column; whereas the acid gas stream with a mole ratio of 0.2 % H_2S to CO_2 may be either sent back to the raw biogas source (e.g., wastewater, landfill or even the digestion unit) or treated separately, since it cannot be directly released to the atmosphere. According to the mentioned process, shown in Figure 5 a, the total energy required by the liquid-feed heat exchanger of the column (EXLA) is equal to the total energy given by the heat exchangers (EXLB) and (HX-NEW2). These heat exchangers have been simulated separately in order to properly analyze the heat balance of the system. In consequence, the additional energy demand for the process are given by the heat exchangers (HX-NEW1) and (HX-NEW2). Similarly, the solvent liquid pumps (P-NEWA) and (P-NEWB) correspond to the same equipment, separated for analysis purposes. The only considered electrical power is however the one reported by (P-NEWA).

Additionally to the considered NRTL thermodynamic model for the equipment from the base case scenario (see Figure 1), simulations of the conceived methanol-based absorption column considered the PC-SAFT thermodynamic model, as recommended by (Papadopoulos and Seferlis, 2017; Sun and Smith, 2013) based on experimental data. The SR-POLAR equation-of-state (EoS) was otherwise used on the constitutive equipment of the solvent feeding units and the refrigeration unit for the methanol solvent. SR-POLAR is an extension of the Soave-Redlich-Kwong EoS reported convenient to work with polar fluids under high pressure, above 5000 kPa (Aspen Technology Inc, 2001).

Chemical absorption with monoethanolamine aqueous solution, $MEA_{(aq)}$, on the other hand, has been suggested in the past by for biogas treatment by several authors, such as (Abdeen et al., 2016; Tippayawong and Thanompongchart, 2013). The main reasons for its application leading to a comparison with the proposed bubble column reactor are:

- $MEA_{(aq)}$ as well as other alkanolamine aqueous solutions are widely used solvents in the petrochemical industry for acid gas removal by chemical absorption. MEA results specially to be the cheapest, nonetheless the most energy consuming from the solvent's family during its regeneration step (Kohl and Nielsen, 1997).

- Several industrial-scale absorption columns working with $MEA_{(aq)}$, normally for natural gas upgrading, are reported to remove impurities up to produce a gas stream with less than 4 ppmv in H_2S and less than 2 % in CO_2 (Kohl and Nielsen, 1997).

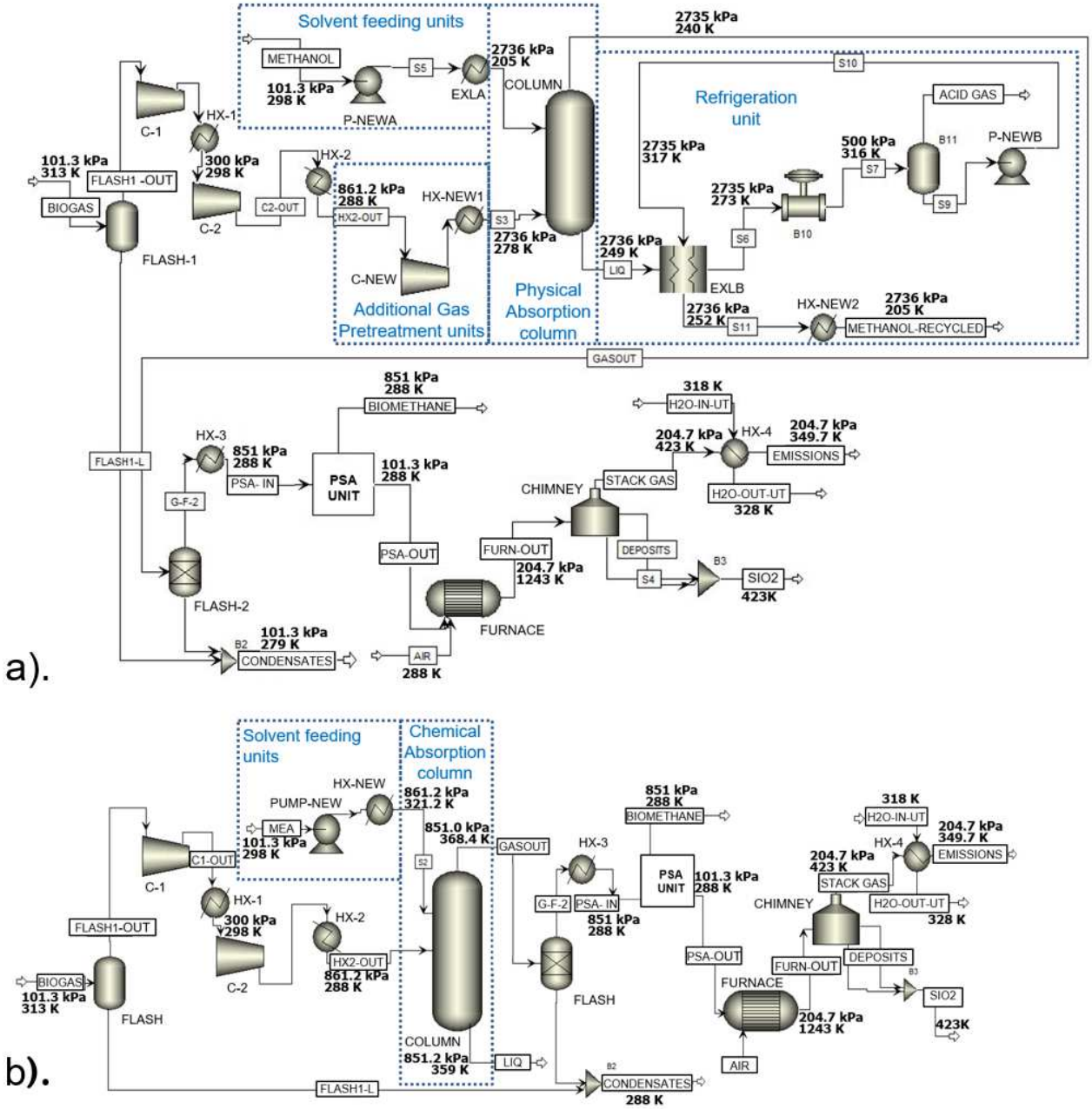

Figure 5. Simulation process diagram (on Aspen Plus V8.6) for the biogas purification process by a). physical absorption with methanol solvent and b). chemical absorption with $MEA_{(aq)}$ solvent

The conceived $MEA_{(aq)}$ purification unit results from a simplification of the regular amine absorption process, using a single absorption column without a regeneration step due to the need an additional column and its high energy requirements. This simplification agrees with the conditions reported by (Tippayawong and Thanompongchart, 2013) for a biogas treatment unit, requiring continuous solvent replacements. The simulation diagram for this process is presented in Figure 5 b. Similar to the process based on the use of methanol solvent, the operating conditions of the process with $MEA_{(aq)}$ were adjusted by maximizing the acid gas elimination and by minimizing the solvent loss within the gas phase.

According to Figure 5 b, biogas purification with $MEA_{(aq)}$ solutions requires two sets of new units. First, the absorption unit conceived and simulated as a packed column by using the

rated-based RadFrac module in Aspen Plus V8.6. This column may operate with 7 theoretical stages, a mixed-flow model and a reactive film resistance (Filmrxn) for both liquid and gas phases. Second, a liquid pump (PUMP-NEW) followed by a heat exchanger (HX-NEW) assuring liquid solvent feed to the column at 861.26 kPa and 321.22 K.

$MEA_{(aq)}$ absorption column was simulated using the ELECNRTL thermodynamic model imposing the contribution of the Henry constant of the gas phase components. This thermodynamic model allows considering ionic interactions resulting from the solubilized gas species and the aqueous solvent solution. On the other hand, AMINES thermodynamic model was implemented for the simulation of the solvent feeding units. AMINES model is based on the Kent-Eisenberg equations, which calculate liquid phase fugacity of the species from equilibrium constant values. This model is normally recommended for processes using solvents with amine functional groups (Aspen Technology Inc, 2001).

Overall comparison between the three processes: the bubble column reaction system with the Superacid 9/1, the physical absorption with methanol and the chemical absorption with MEA(aq) was performed considering the same global conditions as detailed for the base case scenario. The separation objective was to produce biomethane with a CH_4 content of 97 % and a stack gas with SO_2 emission below 100 ppmv, as required by environmental regulations.

4. RESULTS AND DISCUSSION

4.1 Novel purification system design

Table 5 presents the process related results of the novel biogas purification system using of the Superacid 9/1 in a bubble column reactor. Process simulations were performed considering three different conditions of H_2S content in the raw gas: 400, 1000 and 1500 ppmv (dry basis). The novel purification unit was optimized as part of the commonly used biogas process aimed to produce biomethane, establishing a maximum SO_2 content of 100 ppmv in the gas emissions while burning the off-gases occurring from upgrading of biogas. This condition is set by existing environmental regulations, as previously described on this paper.

Table 5. Results of the novel purification process using a bubble column reactor with the "Superacid 9/1" for biogas treatment

H_2S feed concentration (ppmv in dry basis)	**400**	**1000**	**1500**
Reactor operating conditions			
Temperature, T (K)	288.15	288.15	288.15
Pressure, P (kPa)	861.26	861.26	861.26
Solvent flow rate. Q_L (L/s)	10.23	18.75	23.39
Q_G/Q_L ratio (vol./vol.)	1.71	0.93	0.75
Liquid height, H_L (m)	3.20	3.20	3.20
H_L/D ratio	3.37	3.37	3.37
Process efficiency			
H_2S elimination (%)	83.50	94.31	96.41
CO_2 absorbed (%)	58.28	77.78	83.50
Siloxanes absorbed (%)	100	100	100
COVNM absorbed (%)	100	100	100
SO_2 content in the stack gas (ppmv)	99.0	100.1	100.0
CH_4 lost along with the solvent (%)	4.74	8.77	9.54
Solvent lost along with the gas (%)	$2.3 \cdot 10^{-3}$	$1.1 \cdot 10^{-3}$	$0.8 \cdot 10^{-3}$
Solvent feeding pump			
Efficiency (%)	85.0	85.0	85.0
Elec. Power (kW_e)	9.79	18.51	23.00
Recycled solvent cooling system			
Water flow rate at 293.15 K (L/s)	17.54	47.12	51.62
Efficiency (%)	85.0	85.0	85.0
Elec. Power (W_e)	206.4	554.3	607.41

Implementing the bubble column reactor, between the compression units and the PSA unit, with a $Q_G/Q_L < 2$ sets up for the proper gas dispersion in the liquid phase and for the enhancement of the physical absorption of impurities due to the operating high pressure.

Remarkably proven by the tabulated results in Table 5, fixed reactor dimensions and only solvent flow rate adjustments from 10.23 to 23.39 L/s lead to sufficient H_2S elimination from biogas streams with a nominal flow rate of 500 Nm^3/h and a H_2S content between 400 and 1500 ppmv (dry basis). The proposed reactor additionally achieves great reduction of the CO_2 content in the outlet gas, ranging from 58.28 to 83.50 % in function of the solvent flow rate. This performance to CO_2 absorption reduces the separation load for the following PSA unit in the process line until the CO_2 solvent saturation. It may therefore represent cost reductions and most likely enhancements on its performance as compared to the non-feasible CO_2 elimination processes as the currently used activated carbon. Total elimination of siloxanes and NMVOCs were similarly attained with the optimized conditions, which shall physically protect the following process equipment from silicates deposition and possible corrosion issues.

Possible methane loss by solvent absorption is estimated to be lower than 10 % within the bubble column up to the saturation point and for a H_2S maximum concentration of 1500 ppmv (dry basis). This methane slippage can still be lower than 5 % in overall if the dimensions of the reactor are optimized for the highest H_2S content, as it is presented for the base case of 400 ppmv (dry basis). CH_4 additional process losses are frequently given by the absorption in the flash separators and from the PSA unit. On the other hand, solvent evaporation to the gas phase within the bubble column reactor is estimated to be lower than 0.003 %.

Additional energy demands for the operation of the novel bubble column reactor are related to the need of two pumps, one for the recycling system of cooling water and the other one for the pump serving to feed the solvent to the reactor. For a normally considered 85 % pump efficiency, the total needed electrical energy is estimated to be between 10.0 and 23.6 kW_e in function of the previously described solvent flow rate and therefore H_2S content in the feed gas stream.

Concerning the hydrodynamic properties and the bubble column reactor stability, Table 6 presents the results for the describing parameters. Besides the mentioned appropriate values for the Q_G/Q_L ratio, the values for the superficial velocities $U_G < 0.06\,m/s$ and $U_L < 0.2\,m/s$ confirm the targeted bubbly regime within the reactor. Even if the results obtained from the equations by *Zhener (1986)* and by *Riquarts (1981)* diverge, both fall into the design specifications for the equipment, which are specified in Table 5. For the bubble-scale specifications, the obtained values for its mean diameter ($d_b < 0.2\,mm$) for either equation used, from *Moo-Young (1981)* or from *Wilkinson et al. (1994)*, allows considering the formation of mostly spherical gas bubbles within the liquid phase. These results are however complementary to the bubble aspect ratio values ($AR_b < 1$) values as defined by experimental results from (Besagni et al., 2018) and the virtual mass coefficient ($C_{vm} = 0.7 - 1.5$) values; both representing the formation of non-completely spherical but ellipsoidal bubbles. Either spherical or ellipsoidal bubble shapes are recommended for a proper gas dispersion in a liquid; it is noteworthy to avoid the formation of spherical cap-like bubble, which do not refer to a good bubble stability.

Table 6. Results of the hydrodynamic properties for the novel purification process using a bubble column reactor with the "Superacid 9/1" for biogas treatment

Property	Equation (author and No)		H_2S concentration (in dry basis)		
			400 ppmv	1000 ppmv	1500 ppmv
Bubble-scale properties					
U_G (m/s)		(16)	0.016	0.011	0.010
U_L (m/s)	*Zhener (1986)*	(17)	0.198	0.186	0.182
	Riquarts (1981)	(18)	0.060	0.027	0.023
d_b (m)	*Moo-Young (1981)*	(19)	0.0016	0.0016	0.0016
	Wilkinson et al. (1994)	(20)	0.0010	0.0011	0.0011
AR_b (-)		(21)	0.606	0.606	0.606
U_b (m/s)	*Jamialahmadi et al (1991)*	(22)	0.087	0.089	0.090
	D. Darmana (2005)	(23)	0.190	0.190	0.190
C_{vm} **(-)**	*Lance & Bataille (1991)*	(24)	1.400	1.151	1.077
Reactor(equipment)-scale properties					
$\mathcal{E}_G$ (-)	*Joshi & Sharma (1979)*	(25)	0.070	0.034	0.029
	Hughmark (1967)	(26)	0.056	0.026	0.023
	Hikita et al. (1980)	(27)	0.079	0.050	0.046
a_i (m^2/m^3)	*Akita & Yoshida (1980)*	(28)	20.505	8.615	7.356
$K_L a_i$ (s^{-1})	*Shah et al (1982)*	(29)	0.0221	0.0114	0.0101
	Kang et al. (1999)	(30)	0.0015	0.0012	0.0012
ϕ_c (-)		(31)	2.093	0.796	0.738
tr_G (s)		(32)	14.825	15.372	16.284
Industrial-scale properties and dimensionless numbers					
d_b^{max} (m)	*Ishii & Kojasoy (1993)*	(33)	0.074	0.074	0.074
D_H^* (m)	*Rayleigh-Taylor Instability*	(34)	0.30	0.30	0.30
AR_c (-)		(35)	4.42	3.37	3.37
f_I (stability)	*Joshi et al. (2001)*	(36)	0.930	0.769	0.718
E_{DG} (-)		(37)	0.806	0.241	0.193
E_{DL} (-)		(38)	0.203	0.155	0.147
	Hikita & Kikukawa (1974)	(39)	0.220	0.199	0.197
Pe_G (-)		(40)	1.604	2.914	3.414
Pe_L (-)		(41)	1.352	0.584	0.527
$Fr_G \times 10^{-5}$ (-)		(42)	6.32	1.27	9.44
Fr_L (-)		(43)	0.020	0.009	0.008
h_L^{min} (m)		(44)	0.137	0.092	0.085
Bd (-)		(45)	0.325	0.336	0.338
We $\times 10^{-4}$ (-)		(46)	5.96	6.16	6.19

In terms of the industrial-scale properties, the gas holdup ($\mathcal{E}_G$) calculated values are also presented in Table 6. These results correspond to the three different previously described equations: *Joshi & Sharma (1979), Hughmark (1967)* and *Hikita et al. (1980)*. Different values were obtained from each equation, but it is nevertheless confirmed for all the results an $\mathcal{E}_G \leq 15$ % as required for the bubbly regime within the reactor. The results from *Hikita et al. (1980)* were however the ones used for the further estimations requiring this variable, since its definition considers the ionic forces interaction in the dispersion medium. Ionic species were considered for the reactor simulations while setting up the ionic chemical reactions as well as for the overall thermodynamic contributions. This equation from *Hikita et al. (1980)* similarly provides higher values for $\mathcal{E}_G$ than the other relations, indicating therefore a possible high limit value for the design specifications.

Mass transfer parameters, $K_L a_i$ and a_i provided satisfactory values as specified for a bubble column operation, as reported by (J. C. Middleton et al., 1997). First, the referenced interface surface area recommended for bubble columns shall be within the realm of $a_i \sim 20\ m^2/m^3$. Lower values were however obtained as the solvent flow rate increases in the column, which is directly related to the reduction of the total bubbles volume in the liquid phase, i.e., the reduction of the $\mathcal{E}_G$ values. Second, the obtained $K_L a_i$ values for the designed reactors lay into the recommended range, i.e., $K_L a_i = 0.005 - 0.02\ s^{-1}$. This ensures the functioning of the bubble column reactors as per the feedback from experience for similar types of equipment. Finally, the dimensionless time ratio (ϕ_c) values put in evidence the fact that as the solvent flow rate increases, the mixing time becomes dominant in the process as compared to the mass

transfer time. This is similarly related to the effect of lower bubbles volume in the liquid, offering a lower interface surface area. Results for ϕ_c parameter are not to worry about since the optimized mean gas residence time (tr_G) is almost constant for all the cases evaluated, indicating a sufficient time for the coupled effect of the physical and chemical absorption within the reactor.

The industrial-scale stability of the bubble column reactor, potentially facing-up possible process perturbations for the gas and liquid phases, was assured by assessing different design parameters, as shown in Table 5. First, the stability for possible bubbles break-up, resulting from velocity gradients at the interface, required values of $d_b < d_b^{max}$ as confirmed by the results tabulated on the table. Second, the chance of possible bubble formation avoidance, because of the difference of density between the liquid and gas phases, was confirmed by the values obtained for the hydraulic diameter, $D_H^* < 52h_L$. This phenomenon of bubble break-up was explained before in the theory section as a result of the so-called Taylor–Rayleigh instability, which leads to bubbles deformation and break-up as the fluids accelerate through the reactor's height. Similarly, possible bubbles coalescence is supposed to be limited by maintaining the range of the column's aspect ratio (AR_c<5), as proposed by (Besagni et al., 2018). The designed bubble column reactors always respected this criterion. Finally, the obtained results for the stability factor from (Joshi et al., 2001) denoting ($f_l > 0$) allow considering negligible influence or out-of-specification functioning of the reactor in regard to the diffusivity or Reynolds stress, because of possible fluids velocity perturbations. In fact, comparative analysis on the gas-phase axial dispersion coefficient (E_{DG}) and the liquid-phase axial dispersion coefficient (E_{DL}), always showed values of $E_{DG} \gg E_{DL}$, which may reflect that no possible backmixing issues should be expected on the unit's operation at the designed specifications.

Analyses on the relevant dimensionless numbers associated to the unit lead to, firstly, justify that none axial dispersions nor liquid backmixing shall be expected in the liquid or gas phases because of the obtained values for the Peclet numbers, $Pe_G > Pe_L$. Secondly, the simulated conditions shall not lead to an entirely phase separation within the column, and therefore a good contact interface is obtained as noted by the obtained Froude numbers for the gas and liquid phases, Fr_G and Fr_L respectively, since $h_L > h_{L,min}$ for all the designs. Finally, the bubbles stability as part of an ionic mixture in the liquid phase are prevented to break-up as demonstrated by the obtained values for the Bond number (Bd) and the Weber number (We)

4.2 Novel system comparison

Once the bubble column reactor conditions were optimized for the targeted separation and hydrodynamic performances, its use was compared to other available and currently used technologies for purification of combustion gases. Comparison results of the proposed bubble column reactor with the Superacid 9/1 and, the chemical and physical absorption columns with $MEA_{(aq)}$ and methanol respectively are presented in Table 7. These results correspond to the purification required for 500 Nm^3/h raw biogas stream with 400 ppmv of H_2S content. Same tendencies were obtained for higher H_2S concentrations in the feed stream.

Table 7. Overall purification unit comparison for 500 Nm^3/h raw biogas stream with 400 ppmv of H_2S content

Property		Novel process with Superacid 9/1		Physical absorption with methanol		Chemical absorption with $MEA_{(aq)}$	
		Feed	Product	Feed	Product	Feed	Product
Liquid solvent							
Flow rate, Q_L (L/min)		613.51	615.13	44	64.95	29.94	34.96
Concentration (mol %)		77.6	76.9	100	96.26	4.95	5.03
Solvent lost in the gas phase (%)			2.27×10^{-3}		5.49×10^{-3}		11.22
Temperature, T (K)		298.52	303.15	205	248.83	321.22	359.01
Pressure, P (kPa)		861.26	861.26	2735.78	2735.78	861.26	851.13
Gas phase							
Flow rate, Q_G (kmol/h)		21.33	15.59	21.33	18.47	21.33	18.62
Temperature, T (K)		310	304.01	278.15	240.41	310	368.4
Pressure, P (kPa)		861.26	861.26	2735.78	2735.78	861.26	851
CH_4 (mol %)		42.54	55.16	42.54	47.68	42.54	48.71
CO_2 (mol %)		29.34	16.75	29.34	20.85	29.34	10.09
H_2S (ppmv)		399.8	90.27	399.77	92.68	399.8	79.8
NMVOCs (ppmv)		386.25	0.01	386.25	7.26	386.25	322.75
Siloxanes (ppmv)		3.52×10^{-5}	8.85×10^{-18}	3.52×10^{-5}	3.27×10^{-7}	3.52×10^{-5}	4.14×10^{-12}
Solvent (ppmv)			0.009 (H_2SO_4) 847.6 (CH_3COOH)		219.3		6357.98
Equipment properties							
Type		Bubble column reactor		Counter-current packed column		Counter-current packed column	
Packing or regime		Regime Bubbly (20.50 m^2/m^3)		INTX Saddle Plastic 25 mm (984 m^2/m^3)		INTX Saddle Plastic 25 mm (984 m^2/m^3)	
Height, H (m)		3.2		1.47		1.9	
H/D		3.37		1.18		4.8	
CO_2 absorbed (%)		58.28		38.47		70	
H_2S eliminated (%)		83.5		79.93		82.6	
CH_4 lost along with the solvent (%)		4.74		2.97		0.09	
Siloxanes eliminated (%)		100		99.2		89.75	
Additional energy requirements							
Liquid pumps [a]	**Elec. power (W_e)**	9997.6		2250		458.8	
Gas compressors [b]	**Pressure ratio (P_{out}/P_{in})**	-		3.18		-	
	Elec. Power (We)	-		26609		-	
Heat exchanger for the gas phase	**Thermal power (W_{th})**	-		39059		-	
	Elec. Power (W_e)	-		7812 (COP = 5)		-	
Heat exchanger for the liquid phase	**Thermal power (W_{th})**	-		20978		39979	
	Elec. Power (W_e)	-		22878 (COP =0.92)		-	

(a) Pumps efficiency of 85 %. For the process with the Superacid 9/1, the liquid corresponds to the solvent feeding the reactor. For the Methanol - based and the $MEA_{(aq)}$-based processes, the liquid corresponds to the solvent feeding the absorption columns.
(b) Compressor's polytropic efficiency of 75 %.

Results from Table 7 concerning the solvent specifications for the three processes show a higher solvent volume of Superacid 9/1 to be needed as compared to the required methanol and $MEA_{(aq)}$ volumes. Even though, higher solvent volume means larger equipment size, noteworthy the Superacid 9/1 offers the possibility to be recycled and while chemically stabilizing the H_2SO_4 reactive component because of the superacid formation reaction, as described on the theory of this article. Instead, the methanol solvent physically saturates and reduces its absorption capability and the $MEA_{(aq)}$ solvent cannot be easily regenerated at least for the biogas applications, avoiding its recycling as proposed by other authors, for instance, (Tippayawong and Thanompongchart, 2013). The high solvent requirement shown by the bubble column reactor with Superacid 9/1 is however compensated, in advantage for the Superacid 9/1, by its easily attainable operating temperatures (above 273 K) as compared to the methanol-based unit (below 205 K) and by its negligible solvent loss (lower than 2.27×10^{-3} %) as compared to the $MEA_{(aq)}$-based unit showing (around 11 %). These properties traduce into lower concentrations of possible solvent evaporation for the Superacid 9/1 as compared to the other units.

Comparing the three process units, different purification performance was achieved for all the impurities but for H_2S, after setting up the final SO_2 content to a maximum of 100 ppmv. This performance, directly dependent on the used solvent volume, was remarkably better for the Superacid 9/1, which is the only unit to completely eliminate simultaneously the NMVOCs and the siloxanes in the gas. Lower siloxanes degradation and NMCVOs elimination was obtained with the $MEA_{(aq)}$ the methanol as solvents.

Concerning the process unit dimensions, the bubble column reactor design requires a bigger volume for the bubbling gas dispersion operation. These dimensions, specified in Table 7, allow classifying the process units in terms of its volume as following:

Volume: Superacid 9/1 > Methanol > $MEA_{(aq)}$.

On the other hand, regarding the estimated energy requirements, based on the data tabulated on Table 7, the bubble column reactor shows the lowest energy requirement. Setting to use this unit requires only 2 recirculating pumps to feed the solvent into the unit and to cool it down with utility water. The energy required by a refrigeration unit and a compressor for the physical absorption with methanol, as well as the need of an energy consuming heat exchanger to warm up the $MEA_{(aq)}$ solvent, renders these systems less attractive for biogas treatment. In wake of this, the units can be classified based on its energy demands as following:

Energy demands: Methanol > $MEA_{(aq)}$ > Superacid 9/1

Besides the described separation performance and energy demands, the bubble column reactor operated with the Superacid 9/1 may be attractive for biogas purification because of its ability to produce stable elemental sulfur with the H_2S from the gas as by product. The absorption with methanol requires accommodating for an additional stabilization unit for treating the sulfur initially absorbed from the gas. The absorption with $MEA_{(aq)}$, on the other hand, requires accommodate for the for a safe disposal system and procedure for the used alkanolamine solutions. Important to highlight is that the methane losses calculated in this work for MEA solvent are lower than potentially expected. This is based on experimental data presented by (Carroll et al., 1998). The latter leads to the conclusion that the Superacid 9/1 solvent has acceptable solubility of methane in the liquid phase and can be a challenger against conventional amine solvents.

It is however important recognizing the limitations of the proposed novel system. Metrology concerns shall be addressed while working with inorganic acids as solvents: $H_2SO_{4(aq)}$ and CH_3COOH. High operation unit volume shall be considered for a proper separation performance. An economic feasibility study is finally recommended once deciding for the best biogas purification treatment unit.

5. CONCLUSIONS

A novel purification system is proposed for raw biogas streams. This system consists on a bubble column reactor equipped with a solvent mixture of sulfuric acid ($H_2SO_{4(aq)}$, ≥ 95.0 wt. %) and acetic acid glacial (CH_3COOH, ≥99.8 vol. %), both commercial grade. A mixture of these acids in a molar ratio of 9/1 for $H_2SO_{4(aq)}$/ CH_3COOH respectively, offers physico-chemical properties within the realm of superacids. Sufficient physical absorption capabilities from each acid solvent as well as its specific reactions with gas impurities allow eliminating H_2S, reducing CO_2 content, and completely degrading siloxanes and NMVOCs from raw biogas streams simultaneously.

Process modeling and simulations for implementing the bubble column reactor within frequently used biogas processes led to propose a unit of 3.2 m height and 3.37 height/diameter ratio. These dimensions allow properly treating around 500 Nm^3/h of raw biogas with H_2S

concentrations between 400 and 1500 ppmv, by adjusting the solvent volume flow between 10.23 and 23.39 L/min.

Proper gas dispersion within the bubble column reactor was study based on different reported stability criteria, for the bubble-scale, reactor-scale and industrial scale operation point of view. Possible issues related to bubbles break-up, liquid solvent backmixing and limitation of the mass transfer between the phases were numerically addressed to be avoided. These numerical relations are a priori validated for bubble column operating conditions using different solvents. On the other hand, liquid and gas physicochemical properties and reactions have been separately validated for specific applications. In consequence, experimental work is however still recommended in order to validate the overall biogas treatment by using the superacid solvent.

Comparison of the proposed system with other absorption-based systems, usually recommended for biogas treatment, was developed. The technologies considered are the physical absorption with methanol and the chemical absorption with $MEA_{(aq)}$ alkanolamine solution. In terms of the systems performance for a targeted final SO_2 concentration in the end of the process, the bubble column reactor is the unit exhibiting best CO_2 absorption property and the only unit capable of completely eliminating siloxanes and NMVOCs simultaneously. Larger column volumes are however required, but significant energy demand reduction is also achieved with the novel system. Attention in the metrology design of unit using this technology is nevertheless recommended.

AUTHOR INFORMATION

Corresponding Author

*Phone: +33-169191729. Email: rodrigo.rivera_tinoco@mines-paristech.fr

Author Contributions

The manuscript was written through contributions of all authors. All authors have given approval to the final version of the manuscript.

References

Abdeen, F.R.H., Mel, M., Jami, M.S., Ihsan, S.I., Ismail, A.F., 2016. A review of chemical absorption of carbon dioxide for biogas upgrading. Chinese J. Chem. Eng. 24, 693–702. https://doi.org/10.1016/j.cjche.2016.05.006

Angelidaki, I., Treu, L., Tsapekos, P., Luo, G., Campanaro, S., Wenzel, H., Kougias, P.G., 2018. Biogas upgrading and utilization: Current status and perspectives. Biotechnol. Adv. 36, 452–466. https://doi.org/10.1016/j.biotechadv.2018.01.011

Arrhenius, K., Magnusson, B., Sahlin, E., 2011. Impurities in biogas: Validation of methodology of analysis for siloxanes, Rapport SGC 243.1102-7371. Svenskt Gastekniskt Center (SGC), Malmö, Sweden.

Aspen Technology Inc., 2014. Aspen Plus V8.6. Aspen Physical Property System.

Aspen Technology Inc., 2013. Rate-Based Model of the CO2 Capture Process by DEA using Aspen Plus, Software Engineering Documentation. Bedford, MA, USA.

Aspen Technology Inc, 2001. Aspen Physical Property System, Software Engineering Documentation. Cambridge, MA, USA.

Averill, B.A., Eldredge, P., 2012. Principles of General Chemistry: The Chemistry of Acid Rain [WWW Document]. URL https://2012books.lardbucket.org/books/principles-of-general-chemistry-v1.0/s08-07-the-chemistry-of-acid-rain.html (accessed 10.7.17).

Awe, O.W., Zhao, Y., Nzihou, A., Minh, D.P., Awe, O.W., Zhao, Y., Nzihou, A., Minh, D.P., Lyczko, N., 2017. A Review of Biogas Utilisation, Purification and Upgrading Technologies. Waste and Biomass Valorization 8, 267–283. https://doi.org/https://doi.org/10.1007/s12649-016-9826-4

Ballaguet, J.-P., Vaidya, M.M., Charry-Prada, I.D., Duval, S.A., 2018. Enhancement of Claus Tail Gas treatment by sulfur dioxide-selective membrane technology. US Patent number: 10,106,410 B2.

Bansal, R.C., Goyal, M., 2005. Activated Carbon Adsorption, 1st ed. CRC Press, Boca Raton, FL, USA.

Bernard, J., 2013. Traitement des effluents sulfurés [WWW Document]. Web page Process. URL http://processs.free.fr/Pages/VersionClassique0.php?page=6213 (accessed 1.29.16).

Besagni, G., Inzoli, F., Ziegenhein, T., 2018. Two-Phase Bubble Columns: A Comprehensive Review. ChemEngineering - Open Access J. 2, 13. https://doi.org/10.3390/chemengineering2020013

Borisov, S.N., M. G. Voronkov, E., Lukevits, Y., 1971. Chapter 2: Organosilicon Derivatives of Sulfur, in: Organosilicon Derivatives of Phosphorus and Sulfur. Springer US, pp. 157–343.
Boulinguiez, B., Le Cloirec, P., 2011. Purification de biogaz. Élimination des COV et des siloxanes. Énergies | Ressources énergétiques Stock. - Tech. l'ingénieur. Réf BE8560.
Bravo, J.L., Rocha, J.A., 1985. Mass transfer in gauze packings. Hydrocarb. Process. January.
Cadena, F., Peters, R.W., 1988. Evaluation of chemical oxidizers for hydrogen sulfide control. J. Water Pollut. Control Fed. 60, 1259–1263.
Carroll, J.J., Jou, F., Mather, A.E., Otto, F.D., 1998. The Solubility of Methane in Aqueous Solutions of Monoethanolamine, Diethanolamine and Triethanolamine. Can. J. Chem. Eng. 76, 945–951. https://doi.org/10.1002/cjce.5450760512
Charry-Prada, I.D., Rivera-Tinoco, R., Bouallou, C., 2017. Methyl Mercaptan Absorption Study into a Hybrid Solvent Mixture Composed of Diethanolamine/Methanol/Water at Temperatures from 313.9 to 353.0 K. Ind. Eng. Chem. Res. 56, 14410–14418. https://doi.org/10.1021/acs.iecr.7b02712
ChemEssen-Inc., 2017. Predicted properties of C2H8O8S2Si - ChemRTP (Chemical Real-Time Predictor for Extensive Chemical Properties).
Cherif, H., 2016. Study and modeling of separation methods of H2S from methane. PSL Research University - MINES ParisTech.
Clément, L., 2016. Traitement du Biogaz: solutions , résultats et intérêt économique [WWW Document]. ATEE. URL http://atee.fr/sites/default/files/ATEE/Fichiers/9-_l_clement_verdesis.pdf (accessed 12.15.16).
Conant, J.B., Hall, N.F., 1927. A study of superacid solutions. II. A chemical investigation of the hydrogen-ion activity of acetic acid solutions. J. Am. Chem. Soc. 49, 3062–3070. https://doi.org/10.1021/ja01411a011
Crapanzano, L., 2008. Polymorphism of sulfur: Structural and Dynamical Aspects. Université Joseph-Fourier - Grenoble I, Grenoble, France.
Cypryk, M., Apeloig, Y., 2002. Mechanism of the acid-catalyzed Si-O bond cleavage in siloxanes and siloxanols. A theoretical study. Organometallics 21, 2165–2175. https://doi.org/10.1021/om011055s
Darmana, D., Deen, N.G., Kuipers, J.A.M., 2005. Detailed modeling of hydrodynamics, mass transfer and chemical reactions in a bubble column using a discrete bubble model. Chem. Eng. Sci. 60, 3383–3404. https://doi.org/10.1016/j.ces.2005.01.025
Deckwer, W.-D., 1985. Design and Simulation of Bubble Columns, in: Lasa, H.I. de (Ed.), Chemical Reactor Design and Technology. Series E: Applied Sciences - No. 110. NATO ASI Series, Ontario, Canada.
Deckwer, W.D., Schumpe, A., 1993. Improved tools for bubble column reactor design and scale-up. Chem. Eng. Sci. 48, 889–911. https://doi.org/10.1016/0009-2509(93)80328-N
Deublein, D., Steinhauser, A., 2010. Biogas from Waste and Renewable Resources: An Introduction, 2nd ed. WILEY-VCH Verlag GmbH Co. KGaA, Deggendorf, Germany. https://doi.org/10.1002/9783527632794
Eimer, D.A., 2014. Gas treating. Absorption theory and practice, 1st ed. WILEY, Chichester, United Kingdom.
European Biogas Association (EBA), 2017. Annual Statistical Report 2017, Abridged version. Brussels, Belgium.
European Commission, 2015. ENVIRONMENT - Air Quality Standards [WWW Document]. URL http://ec.europa.eu/environment/air/quality/standards.htm (accessed 2.12.16).
Fair, J.R., Steinmeyer, D.E., Penney, W.R., Crocker, B.B., 1999. Section 14: Gas Absorption and Gas-Liquid System Design, in: Perry's Chemical Engineers' Handbook Handbook. McGraw-Hill Companies, Inc., pp. 14.1-14.98. https://doi.org/10.1016/S0029-5493(99)00078-3
Flowers, R.H., Gillespie, R.J., Robinson, E.A., 1963. The sulphuric acid solvent system: Part V. Solutions of some organosilicon compounds. Can. J. Chem. 41, 2464–2471. https://doi.org/10.1139/v63-363
Ford, S., 2007. Advances in Biogas, 1st ed. Pira International Ltd, Surrey, UK.
Garci□a, M., Prats, D., Trapote, A., 2015. Presence of Siloxanes in the Biogas of a Wastewater Treatment Plant Separation in Condensates and Influence of the Dose of Iron Chloride on its Elimination. Int. J. Waste Resour. 6, 1–6. https://doi.org/10.4172/2252-5211.1000192
Hansen, C.M., 2007. Hansen Solubility Parameters. A User's Handbook, 2nd ed, Angewandte Chemie International Edition. CRC Press, New York, USA. https://doi.org/10.1201/9781420006834
Hikita, H., Asai, S., Tanigawa, K., Segawa, K., Kitao, M., 1980. Gas hold-up in bubble columns. Chem. Eng. J. 20, 59–67. https://doi.org/10.1016/0300-9467(80)85006-4
Huertas, J.I., Giraldo, N., Izquierdo, S., 2011. Removal of H2S and CO2 from Biogas by Amine Absorption., in: Markoš, J. (Ed.), Mass Transfer in Chemical Engineering Processes. InTech, Monterrey, Mexico, pp. 133–150. https://doi.org/10.5772/20039
J. C. Middleton, Harnby, N., Nienow, A.W., Edwards, M.F., 1997. Chapter 15: Gas-liquid dispersion and mixing, in: Mixing in the Process Industries. Butterworth-Heinemann, Oxford, UK, UK, p. 432. https://doi.org/10.1016/0032-5910(93)80032-6
Jamialahmadi, M., Muller-Steinhagen, H., 1990. Effect of electrolyte concentration on bubble size and gas hold-up in bubble columns. Chem. Eng. Res. Des. 68, 16–31.
Joshi, J.B., Deshpande, N.S., Dinkar, M., Phanikumar, D.V., 2001. Hydrodynamic stability of multiphase reactors, in: Advances in Chemical Engineering. Volume 26. Academic Press, Mumbai, India, pp. 1–130.
Kantarci, N., Borak, F., Ulgen, K.O., 2005. Bubble column reactors. Process Biochem. 40, 2263–2283. https://doi.org/10.1016/j.procbio.2004.10.004
Kerber, J., Repke, J.U., 2016. Mass transfer and selectivity analysis of a dense membrane contactor for upgrading biogas. J. Memb. Sci. 520, 450–464. https://doi.org/10.1016/j.memsci.2016.08.008
Kirk, R.E., Othmer, D.F., Grayson, M., Eckroth, D., 2000. Mass Transfer, in: Kirk-Othmer Encyclopedia of Chemical Technology. Wiley-Interscience. John Wiley & Sons Inc., New Jersey, USA, pp. 1–75. https://doi.org/10.1002/0471238961
Kohl, A., Nielsen, R., 1997. Gas Purification, 5th ed, Gas Purification. Gulf Publishing Company, Houston, Texas. https://doi.org/10.1016/B978-088415220-0/50009-4
Kolev, N.I., 2005. Drag, lift, and virtual mass forces, in: Multiphase Flow Dynamics 2. Mechanical Interactions. Springer Berlin Heidelberg, Herzogenaurach, Germany, Germany, pp. 31–86. https://doi.org/10.1007/978-3-642-20598-9
Kotov, A. V., Zarinskii, V.A., Bokina, V.M., 1969. Mechanism of the interaction of concentrated sulfuric acid and glacial acetic acid. Bull. Acad. Sci. USSR Div. Chem. Sci. 18, 1319–1322. https://doi.org/10.1007/BF00908172
Krischan, J., Makaruk, A., Harasek, M., 2012. Design and scale-up of an oxidative scrubbing process for the selective removal of hydrogen sulfide from biogas. J. Hazard. Mater. 215–216, 49–56. https://doi.org/10.1016/j.jhazmat.2012.02.028
Largitte, L., Pasquier, R., 2016. A review of the kinetics adsorption models and their application to the adsorption of lead by an activated carbon. Chem. Eng. Res. Des. 109, 495–504. https://doi.org/10.1016/j.cherd.2016.02.006
Lewkiewicz-Malysa, A., Rogowska-Kwas, R., Winid, B., 2008. Reduction of hydrocarbon contaminations in the chemical oxidation process. Czas. Tech. 249–256. https://doi.org/ISSN: 0011-4561

Lopez de Bertodano, M., Lahey, R.T., Jones, O.C., 1994. Phase distribution in bubbly two-phase flow in vertical ducts. Int. J. Multiph. Flow 20, 805–818. https://doi.org/10.1016/0301-9322(94)90095-7
Majumder, S.K., 2016. Hydrodynamics and Transport Processes of Inverse Bubbly Flow, 1st ed, Hydrodynamics and Transport Processes of Inverse Bubbly Flow. Elsevier Inc., Amsterdam, Netherlands. https://doi.org/10.1016/B978-0-12-803287-9.00007-2
Marriott, R.A., Pirzadeh, P., H, J.J.M., Raval, S., Marriott, R.A., 2016. Hydrogen Sulfide Formation in Oil and Gas. Can. J. Chem. 94, 406–413.
Methanol Institute (MI), 2016. Methanol Technical Data Sheet (MSDS). Washington, DC 20460.
N. Madox, R., 1982. Gas Conditioning and Processing, 3rd ed. Campbell Petroleum Series, Norman, Oklahoma 73069, U.S.A.
Naskeo Environment, 2009. Biogas Renewable Energy - Information website on biogas [WWW Document]. URL http://www.biogas-renewable-energy.info/index.html (accessed 1.1.16).
Nedeltchev, S., 2017. Theoretical prediction of mass transfer coefficients in both gas–liquid and slurry bubble columns. Chem. Eng. Sci. 157, 169–181. https://doi.org/10.1016/j.ces.2016.06.047
Nexant-Chem systems, 2006. Gas Processing and NGL Extraction: Gas Conditioning PERP 04/05S8. Nexant PERP REPORT, New York 10601, USA.
Nielsen, A.H., Vollertsen, J., Hvitved-Jacobsen, T., 2006. Kinetics and stoichiometry of aerobic sulfide oxidation in wastewater from sewers-effects of pH and temperature. Water Environ. Res. 78, 275–283. https://doi.org/10.2175/106143005x94367
Olah, G.A., Prakash, G.K.S., Molnar, Á., Sommar, J., 2009. Superacid Chemistry, 2nd ed, John Wiley & Sons, Inc. WILEY - John Wiley & Sons, Inc., Hoboken, New Jersey, USA. https://doi.org/10.1002/9780470421604
Papadopoulos, A.I., Seferlis, P., 2017. Process Systems and Materials for CO2 Capture Modelling, Design, Control and Integration, 1st ed. WILEY - John Wiley & Sons, Inc., Thessaloniki, Greece. https://doi.org/10.1002/9781119106418
Ricaurte Ortega, D., 2009. Étude Du Traitement Des Siloxanes Par Adsorption Sur Matériaux Poreux : Application Au Traitement Des Biogaz. PhD Thesis Dissertation (Thèse de Doctorat en Génie des Procédés), Université de Nantes, France, Nantes, France.
Roman, P., 2016. Biotechnological removal of H2S and thiols from sour gas streams under haloalkaline conditions. PhD Thesis.
Ruiling, G., Shikun, C., Zifu, L., 2017. Research progress of siloxane removal from biogas. Int. J. Agric. Biol. Eng. 10, 30–39. https://doi.org/10.3965/j.ijabe.20171001.3043
Rumpf, B., Xia, J., Maurer, G., 1998. Solubility of Carbon Dioxide in Aqueous Solutions Containing Acetic Acid or Sodium Hydroxide in the Temperature Range from 313 to 433 K and at Total Pressures up to 10 MPa. Ind. Eng. Chem. Res. 37, 2012–2019. https://doi.org/10.1021/ie9706626
Sarrafi, A., 1999. Gas holdup in homogeneous and heterogeneous gas—liquid bubble column reactors. Can. J. Chem. Eng. 77, 11–21. https://doi.org/10.1002/cjce.5450770104
Shah, Y.T., Kelkar, B.G., Godbole, S.P., Deckwer, W.-D., 1982. Review: Design parameters estimations for bubble column reactors. AIChE J. 28, 353–379. https://doi.org/10.1002/aic.690280302
Shah, Y.T., Stiegel, G.J., Sharma, M.M., 1978. Backmixing in gas-liquid reactors. AIChE J. 24, 369–400. https://doi.org/10.1002/aic.690240302
Siang, H.Y., Tahir, N.M., Malek, A., Isa, M.A.M., 2017. Breakdown of hydrogen sulfide in seawater under different ratio of dissolved oxygen/hydrogen sulfide. Malasysian J. Anal. Sci. 21, 1016–1027.
Smith, J.M., Van Ness, H.C., Abbott, M.M., 2005. Introduction to Chemical Engineering Thermodynamics, 7th ed. Mc Graw-Hill's Chemical Engineering Series, New York, NY 10020.
Soreanu, G., Béland, M., Falletta, P., Edmonson, K., Svoboda, L., Al-Jamal, M., Seto, P., 2011. Approaches concerning siloxane removal from biogas - A review. Can. Biosyst. Eng. 53, 8.1-8.18.
Sun, L., Smith, R., 2013. Rectisol wash process simulation and analysis. J. Clean. Prod. 39, 321–328. https://doi.org/10.1016/j.jclepro.2012.05.049
Swedish Gas Centre, 2012. Basic Data On Biogas, Swedish Gas Technology Centre Ltd (SGC). Malmo, Sweden. https://doi.org/ISBN 978-91-85207-7
Tansel, B., Surita, S.C., 2014. Oxidation of siloxanes during biogas combustion and nanotoxicity of Si-based particles released to the atmosphere. Environ. Toxicol. Pharmacol. 37, 166–173. https://doi.org/10.1016/j.etap.2013.11.020
Tilton, J.N., 2008. Section 6: Fluid and Particle Dynamics, in: Perry's Chemical Engineers' Handbook. McGraw-Hill Companies, Inc., pp. 6.1-6.54. https://doi.org/10.1036/0071511296
Tippayawong, N., Thanompongchart, P., 2013. Biogas quality upgrade by simultaneous removal of CO2 and H2S in a packed column reactor. Songklanakarin J. Sci. Technol. 35, 683–691. https://doi.org/10.1016/j.energy.2010.04.014
Vienna University of Technology, 2012. Du Biogaz Au Biomethane - Revue Technique, Rapport dans le cadre du Projet Europeen Bio-méthane regions et du programme Energie Intelligente Europe. Intellignet Energy Europe, Vienna, Austria.
Wang, H., Dalla Lana, I.G., Chuang, K.T., 2002a. Kinetics and Mechanism of Oxidation of Hydrogen Sulfide by Concentrated Sulfuric Acid. Ind. Eng. Chem. Res. 41, 6656–6662. https://doi.org/10.1021/ie0200407
Wang, H., Lana, I.G.D., Chuang, K.T., 2002b. Kinetics of Reaction between Hydrogen Sulfide and Sulfur Dioxide in Sulfuric Acid Solutions. Ind. Eng. Chem. Res. 41, 4707–4713. https://doi.org/10.1021/ie020275i
Wu, Y., Al-Dahhan, M.H., 2001. Prediction of axial liquid velocity profile in bubble columns. Chem. Eng. Sci. 56, 1127–1130. https://doi.org/10.1016/S0009-2509(00)00330-4
Zhang, Q., Lana, I.G.D., Chuang, K.T., Wang, H., 2000. Reactions between Hydrogen Sulfide and Sulfuric Acid : A Novel Process for Sulfur Removal and Recovery. Ind. Eng. Chem. Res. 39, 2505–2509. https://doi.org/10.1021/ie990717z

BIOGAS PROCESSING

- ✓ *Process simulations*
- ✓ *Hydrodynamic stability*
- ✓ *Feasibility study*